

Contents lists available at ScienceDirect

Corrosion Science

journal homepage: www.elsevier.com/locate/corsci



Comparative studies of Tris-HCl, HEPES and NaHCO₃/CO₂ buffer systems on the biodegradation behaviour of pure Zn in NaCl and SBF solutions



Xiao Liu^a, Hongtao Yang^b, Pan Xiong^a, Wenting Li^b, Her-Hsiung Huang^c, Yufeng Zheng^{a,b,*}

- ^a Academy for Advanced Interdisciplinary Studies, Peking University, Beijing 100871, China
- ^b Department of Materials Science and Engineering, College of Engineering, Peking University, Beijing 100871, China
- ^c Department of Dentistry, National Yang-Ming University, No. 155, Sec. 2, Li-Nong Street, Taipei, Taiwan, China

ARTICLE INFO

Keywords:

A. Zinc

- C. Biodegradation
- C. Simulated body fluid
- C. Buffer system

ABSTRACT

The influence of solution pH and buffer system on the degradation behaviour of pure Zn was investigated and in vitro methodology that can better simulate in vivo corrosion was explored. Electrochemical approaches and immersion tests were performed in buffered pseudo-physiological solutions. It revealed that solution pH affected the degradation and can be adjusted by Tris-HCl, HEPES and $NaHCO_3/CO_2$. The pH-control ability and associated influence of three buffer systems varied in NaCl solution and SBF, owing to the introduction of different inorganic ions. Tris-HCl and $NaHCO_3/CO_2$ buffered SBF were recommended for future evaluation of biodegradation behaviour of Zn and its alloys.

1. Introduction

As a new generation of metallic biomaterials, biodegradable metals have received noticeable attention due to superior mechanical properties to that of biodegradable polymers and potential applications in cardiovascular intervention and bone repair [1]. Zn, an essential element in human bodies, is recently suggested as a promising alternative to magnesium-based and iron-based materials [2], and expected to degrade at a suitable rate satisfying the clinical requirements for ideal bioabsorbable materials [2]. So far, there are several reports performing in vitro and in vivo experiments on biodegradable zinc and zinc-based alloys [3-6]. A number of electrolytes such as 0.9 wt.% NaCl solution [7], simulated body fluid (SBF) [8-11], Hanks' solution [12-14], phosphate buffered saline (PBS) [15,16] and Ringer's saline solution [16] are used as test media in vitro. However, the disparity of degradation behaviour between in vivo and in vitro is unveiled [17], which is a point of contention and makes the material characterization in vitro less credible. In physiological environment, the degradation of implants is synergistically affected by inorganic ions, organic molecules, proteins, cells, temperature, localized pH value and O2 concentration [18]. Therefore, to find a more reliable corrosive medium for in vitro tests, it's necessary to carefully and systematically analyse the impact of individual component and clarify their synergistic effects to thoroughly understand the corrosion performance of zinc in vivo.

In the physiologically environment, pH of tissue fluid is critical for

the normal function of proteins and cells [19]. The deep change of acidbase balance can cause the disruption of protein structure and the loss of normal function [19]. In the field of degradable metals, pH values influence the formation and dissolution of corrosion product. The Pourbaix diagram calculated by Bowen et al. for Zn-H₂O and Zn-X-H₂O systems revealed the pH-dependence of corrosion product formed during Zn dissolution, such as ZnO, ZnCO3 and ZnP [20]. In the pH range from 7.7 to 11, ZnO is thermodynamically stable. In the physiological range, ZnO becomes instable and other corrosion products tend to precipitate [21]. When exposed to simple simulated body fluids, pH value increases gradually owing to by-product OH of the dissolution of zinc. In contrast, the pH level in human body is sustained within the range from 7.35 to 7.45 [22]. The pH variations are likely to introduce discrepancies of degradation behaviour and corrosion product. The maintenance of a specific pH range in vitro is therefore crucial for the evaluation of degradation.

The pH level in human body is controlled by the natural buffer system, which is mainly comprised of HCO_3^- (~27 mmol/L), HPO_4^{2-} (~1 mmol/L) and plasma protein buffers (~17 mmol/L) [23]. Similarly, the control of pH in vitro can be achieved through an appropriate buffer. Tris (hydroxymethyl) aminomethane buffer (Tris-HCl) and 4-(2-hydroxyethyl)-1-piperazineethanesulfonic acid (HEPES), which cannot be traced in human body, are found to be promising candidates in biological studies [24]. Together with NaHCO $_3$ /CO $_2$ buffer, as well as phosphate buffer solution (PBS) and borate buffer solution (BBS), five

^{*}Corresponding author at: Department of Materials Science and Engineering, College of Engineering, Peking University, Beijing 100871, China. E-mail address: yfzheng@pku.edu.cn (Y. Zheng).

Table 1The chemical composition of plasma and electrolytes used in this study (mmol/L).

	Human Plasma	NaCl	NaCl+ Tris-HCl	NaCl + HEPES	NaCl+ NaHCO ₃ /CO ₂	SBF	SBF+ Tris-HCl	SBF+ HEPES	SBF+ NaHCO ₃ /CO ₂
Na+	142	154	154	154	180	142	142	142	164
K ⁺	5.0	_	-	-	_	5.0	5.0	5.0	5.0
Mg ²⁺	1.5	-	-	-	-	1.5	1.5	1.5	1.5
Ca ²⁺	2.5	-	-	-	-	2.6	2.6	2.6	2.6
Cl-	103	154	> 154	154	154	149	> 149	149	149
HCO ₃ -	27.0	-	-	-	26.2	4.2	4.2	4.2	26.2
HPO ₄ ²⁻	1.0	-	-	-	-	1.0	1.0	1.0	1.0
SO ₄ ²⁻	0.5	_	_	_	_	0.5	0.5	0.5	0.5
Tris	_	_	50.5	-	-	_	50.5	-	_
HEPES	_	-	_	25.0	_	_	_	25.0	-

buffer systems have been frequently used for in vitro studies of biodegradable magnesium [25,26].

In the human body, bicarbonate ions produced by the oxidation of organic molecules could provide the buffer capacity. Thereupon, the NaHCO $_3$ /CO $_2$ buffer is generally recommended [27]. The mixture of NaHCO $_3$ in solution and controlled partial CO $_2$ atmosphere establishes the HCO $_3$ $^-$ /H $_2$ CO $_3$ buffer system [28] and determines the buffering capacity [29]. Typically, 2.2 g/L NaHCO $_3$ and 5% CO $_2$ can meet requirements. The pH-control ability was confirmed in several studies of biodegradable magnesium [27,30,31]. Walker et al. [30] demonstrated that degradation rates of pure Mg and five magnesium alloys in Earle's balanced salt solution (EBSS) buffered with NaHCO $_3$ were comparable to in vivo results. Abidin et al. [32] claimed that Nor's solution, a combination of Hank's solution and bubbled CO $_2$, was feasible to predict the degradation of magnesium alloy in vivo [22]. Even so, the application of NaHCO $_3$ /CO $_2$ is limited due to complex requirements for equipment and operations.

The HEPES and Tris-HCl buffer systems are promoted for experimental simplicity, which are atmosphere-independent and provide appropriate buffering capacity without any special requirements [27]. HEPES is a zwitterion buffer and widely used in the cell culture medium [33]. It covered a wide pH range from 6.8 to 8.2 and can neutralize an excess number of protons to limit the magnitude of surface acidification [34]. Usually, 5.96 g/L (25 mmol/L) HEPES is required to constitute the buffer system [35,36]. Tris-HCl buffer has the ability maintaining a larger pH range from 7.0 to 9.0 [37]. The hydrolysis of the amino-group of Tris raises pH value [34], bonded H⁺ in Tris-HCl consumes generated OH⁻ [38] and pH values is thus adjusted.

Although the buffer system plays a pivotal role in keeping a defined pH value, the interactions between the buffering agent and the Zn surface raise concerns. It's reported that HEPES in EBSS inhibited the formation of insoluble salt layer and accelerated magnesium degradation [29]. Tris-HCl retarded the deposition of corrosion products, promoted the dissolution of magnesium [38] and increased corrosion rate [34]. Besides, increased Cl⁻ concentration from Tris-HCl was far from the physiological environment [27] and might alter corrosion mode and raise corrosion rates. To date, no investigation has introduced buffer systems into the research of biodegradation Zn systematically. Selection of an optimum buffer system for the in vitro research and elucidation of corresponding impacts on the degradation behaviour of Zn should be put on the agendas.

This work aims to elucidate the effect of pH values and buffer systems on the corrosion behaviour of pure Zn in different simulated body fluids. Simulated body fluid (SBF) is widely adopted to reveal the in vitro corrosion performance of biodegradable metals and contains all the inorganic components in human body fluids [23]. Along with the sodium chloride solution, the relation between inorganic ions and buffer systems can be investigated. Thus, 0.9 wt.% NaCl solution and SBF were chosen as the corrosion media, and three buffer system (NaHCO₃/CO₂, HEPES and Tris-HCl) were added. The immersion test, corrosion product characterization, potentiodynamic polarization, and

Electrochemical Impedance Spectroscopy (EIS) were performed to demonstrate the initial corrosion behaviour of pure Zn in different pseudo-physiological solutions and explain the buffer-Zn interaction.

2. Experimental

2.1. Sample preparation

Pure zinc (99.99 wt.%) used in this study was cut from extruded zinc rods and in the shape of 1 mm thick discs with a 10 mm diameter. The zinc rods were extruded from ingot at 250 °C and at a reduction ratio of 16. Before use, the specimens were successively wet ground with silicon carbide abrasive paper from 800 to 2000 grit, then ultrasonically cleaned for 5 min in acetone and another 5 min in ethanol. Finally, the samples were dried in air under sterile conditions.

2.2. Immersion tests

 $0.9~\rm wt.\%$ NaCl solution and simulated body fluid (SBF) without Tris-HCl buffer system were used as corrosion media, buffered with 6.1181 g/L Tris, $5.96~\rm g/L$ HEPES or $2.2~\rm g/L$ NaHCO $_3$, in accordance with previous studies of biodegradable magnesium. The concentrations of major components in human plasma [39] and eight electrolytes used in this study are summarized in Table 1. All electrolytes were prepared by dissolving electrolyte powder in distilled water with stirring at 37 °C and adjusted the initial pH to 7.40 with NaOH and HCl.

With a ratio of solution volume to surface area at $20 \, \mathrm{mL/cm^2}$, specimens were immersed for 1, 2, 3, 5, 7 and 14 days. The immersion tests conducted in solutions containing Tris-HCl, HEPES, and no buffer system were kept at $37\,^{\circ}\mathrm{C}$ under normal atmospheric conditions. The solutions containing NaHCO $_3$ were under cell culture conditions and the atmosphere was controlled to be $5\%\,\mathrm{CO}_2$ in humidified air. The pH values of eight immersion media were monitored and recorded. The amount of $\mathrm{Zn^{2+}}$ in solutions under 20 multiple dilution was evaluated by Inductively Coupled Plasma Optical Emission Spectrometer (ICP-OES, Optima 5300 DV, Waltham, MA, USA).

After removal from solutions, samples were rinsed in deionized water and dried in air. The corrosion products on the surface were removed by a solution containing 200 g/L CrO₃. Afterward, samples were rinsed in distilled water and ethanol. The weight of samples was determined after drying and the weight loss was calculated. The corrosion rate (mm/yr) was derived according to the following equation in ASTM-G31-12a:

Corrosion rate =
$$(K \times W) / (A \times T \times D)$$
 (1)

Here the coefficient K = 8.76×10^4 , W is the weight loss (g), A is the exposed area to solution (cm²), D is the density of materials (g/cm³) and T is the immersion time (h).

2.3. Corrosion product analysis

An environmental electron microscopy (ESEM, Quanta 200FEG) coupled with energy-disperse spectrometer (EDS) was used to characterize the morphology of corroded surface. Samples after 14 days of immersion were mounted in epoxy resin. The cross section was exposed by grounding transversely with 800, 2000, 5000 and 7000-grit silicon carbide successively and polishing with diamond grinding paste. The cross section was sputtered with gold before imaging with the scanning electron microscope. EDS elemental mappings of Zn, O, C, Ca, P and Cl from cross sections were captured.

X-ray diffraction (XRD) was performed on an X-ray diffractometer (XRD, Rigaku DMA 2400, Japan) with CuK_{α} radiation. The scans were performed continuously from 10° to 90° in 20 at a speed of 4°/min to identify the corrosion product phase. Fourier transform infrared spectroscopy (FTIR, Nicolet Is50) was conducted in 400-4000 cm $^{-1}$ to analyse the chemical constituents. The surface chemistry was determined by an XPS (Axis Ultra, KRATOS ANALYTICAL, Britain) with AlK α radiation. High resolution narrow scanning was conducted to determine the binding states of Zn 2p, Cl 2p, P 2p and Ca 2p.

2.4. Electrochemical tests

The electrochemical behaviour of pure Zn in eight electrolytes was studied with an electrochemical workstation (Autolab, Metrohm, Switzerland). A three-electrode cell with a saturated calomel electrode (SCE) as the reference electrode and a platinum counter electrode was employed. The exposed area of working electrode in contact with the electrolyte was approximately 0.20 cm² and the electrolyte volume was 150 mL. The tests conducted in solution containing NaHCO3 were aerated with pure CO₂ bubbles and the pH difference before and after the test was controlled less than 0.05. The tests in the rest solutions were carried out at 37 °C under normal atmospheric condition. The stability of the open circuit potential (OCP) was previously checked and continuously monitored for 1 h of immersion. The Electrochemical Impedance Spectroscopy (EIS) measurement was carried out by applying 10 mV perturbation to OCP values, in a frequency range from 10^5 Hz to 10^{-2} Hz. The potentiodynamic polarization (PDP) tests were performed at a scanning rate of 1 mV/s. All the measurements were reproduced at least three times to check the reproducibility.

3. Results

3.1. Morphology observation of pure Zn after immersion

The surface morphology of pure zinc immersed in four groups of NaCl solutions for 14 days is shown in Fig. 1a. During 7 days of immersion in NaCl solution, a compact layer covered the greater part of sample surface and clusters of globular white corrosion product dispersed on the rest areas. As immersion time extended to 14 days, pure Zn demonstrated general corrosion and the compact layer was composed of needle-like particles. The EDS spectrum was performed on selected corroded areas to characterize corrosion products. As shown in Table 2, corrosion products in NaCl solution contained Zn, C, O and Cl. In contrast, specimens experienced predominantly uniform corrosion in NaCl solution buffered with HEPES and NaHCO₃/CO₂. A compact layer of corrosion product formed instantly during the first day and its morphology sustained almost the same during the whole immersion. The layers were mainly composed of Zn, C and O. The SEM images of pure Zn exposed to Tris-HCl buffered NaCl solution displayed completely different corrosion mode. Initially, the film formed during sample preparation was corroded and no corrosion product was precipitated. The localized corrosion proceeded significantly with time and resulted in a myriad of pits and holes. It was after 7 days that the corrosion product started to pile up inside the pits and the layer was formed. According to the EDS results, Zn, C, O and Cl were identified on the film and corrosion products. The cross-sectional morphology and EDS elemental mapping of the specimen after 14 days are also shown in Fig. 1. The corrosion product layer was recognized in four NaCl solutions and mainly consisted of Zn and O. The thickness of layer in bufferfree and HEPES buffered NaCl solution was around 10 μm . Thinner corrosion product layer was identified in the presence of NaHCO $_3$ /CO $_2$, with a thickness of $5\,\mu m$. The layer formed in Tris-HCl buffered NaCl solution was the thickest, with a thickness exceeding 30 μm , and the localized feature was identified, corresponding with corroded pits observed in surface morphology.

Fig. 1b shows representative surface morphology of pure Zn immersed in four groups of SBF solutions. After immersion in SBF for 1 day, few white particles were precipitated on the surface. The amount of particles increased with time and coalesce of particles occurred subsequently. After 14 days, the sample surface was covered with corrosion product agglomerates. As shown in Table 3, corroded particles consisted of Zn, O, C, Ca, P and Mg. Similar elemental composition was identified in the substrate, indicating the formation of corrosion product layer even after 1 day. Meanwhile, intact surface morphology was observed in three buffered SBFs, with less corrosion product dispersed on the surface. The corrosion product and substrate also comprised of Zn, O, C, Ca, P and Mg. The corrosion product layer formed in four SBFs after 14 days was indistinguishable under ESEM, although a thin layer of Ca and P was vaguely recognized in SBF and NaHCO₃/CO₂ buffered SBF. It came to the provisional conclusion that corrosion product film might be too thin to be distinguished.

3.2. Characterization of corrosion product after immersion

As depicted in Figs. 2 and 3, XRD, FTIR and XPS were used to investigate the chemical composition of corrosion products on pure Zn after 14 days of immersion in differently buffered NaCl solutions and SREc

For pure Zn in NaCl solution, XRD spectra identified ZnO and Zn₅(OH)₈Cl₂·4H₂O as main crystallized products. In three buffered NaCl solutions, Zn₅(CO₃)₂(OH)₆ were also identified. The FTIR spectra of pure Zn in four NaCl solutions is depicted in Fig. 2b and corresponding bands or species are listed in Table 4. The existence of water molecules [40], O–H bond [41], ${\rm CO_3}^{2-}$ [40,42,43] and Cl- [44] was confirmed. Besides, peaks at 1037, 906, and 735 cm⁻¹ were ascribed to the vibration of Zn-O-H in Zn₅(OH)₈Cl₂·4H₂O [40]. The band in the region of 350 to 600 cm⁻¹ were associated with the translational modes of Zn-O bonds in ZnO [45]. To comprehensively clarify and further confirm the surface chemical composition, XPS was utilized and chemical state of several elements was studied. In Fig. 2c, Zn, O, C and Cl were present in the survey spectra. The curve fits of the Zn 2p3/2 spectra in NaCl solution consisted of two groups, and in the presence of buffer systems, there were three. As shown in Table 5, ZnO and Zn₅(CO₃)₂(OH)₆ can be recognized [46-48]. Meanwhile, there was the peak related to the Zn²⁺ hexa-coordinated by OH- groups and Zn2+ tetra-coordinated by three OH- and one Cl- [49], and the Cl 2p spectrum after deconvolution consisted of two bonds for the Cl, corresponding to Zn₅(OH)₈Cl₂·4H₂O [50] and Na-Cl bonds [49], respectively. The precipitation of Zn₅(OH)₈Cl₂·4H₂O was accordingly unveiled [50,51].

In Fig. 3a, XRD analysis demonstrated the existence of Zn and ZnO in four SBFs. The FTIR spectra of samples in four solutions exhibited similar pattern in Fig.3b, and further revealed the presence of $\rm H_2O$, O–H bonds, $\rm CO_3^{2-}$ and $\rm PO_4^{3-}$ [6,52]. Therefore, zincite, carbonates and phosphates were formed in four SBFs. However, the precise stoichiometry of carbonates and phosphates cannot be easily determined by the interpretation of FTIR analysis and hence XPS was used for further investigation. In Fig. 3c, Zn, O, C, Ca, P and Mg were present in the survey spectra of samples in four SBFs, and the Zn 2p3/2 spectrum exhibited peaks corresponding to ZnO, Zn(OH)₂ [46], Zn₅(CO₃)₂(OH)₆ and Zn₃(PO₄)₂·4H₂O [53,54]. For sample in buffer-free SBF, however, the peaks of Zn had extremely weak intensity. Instead, Ca 2p spectra

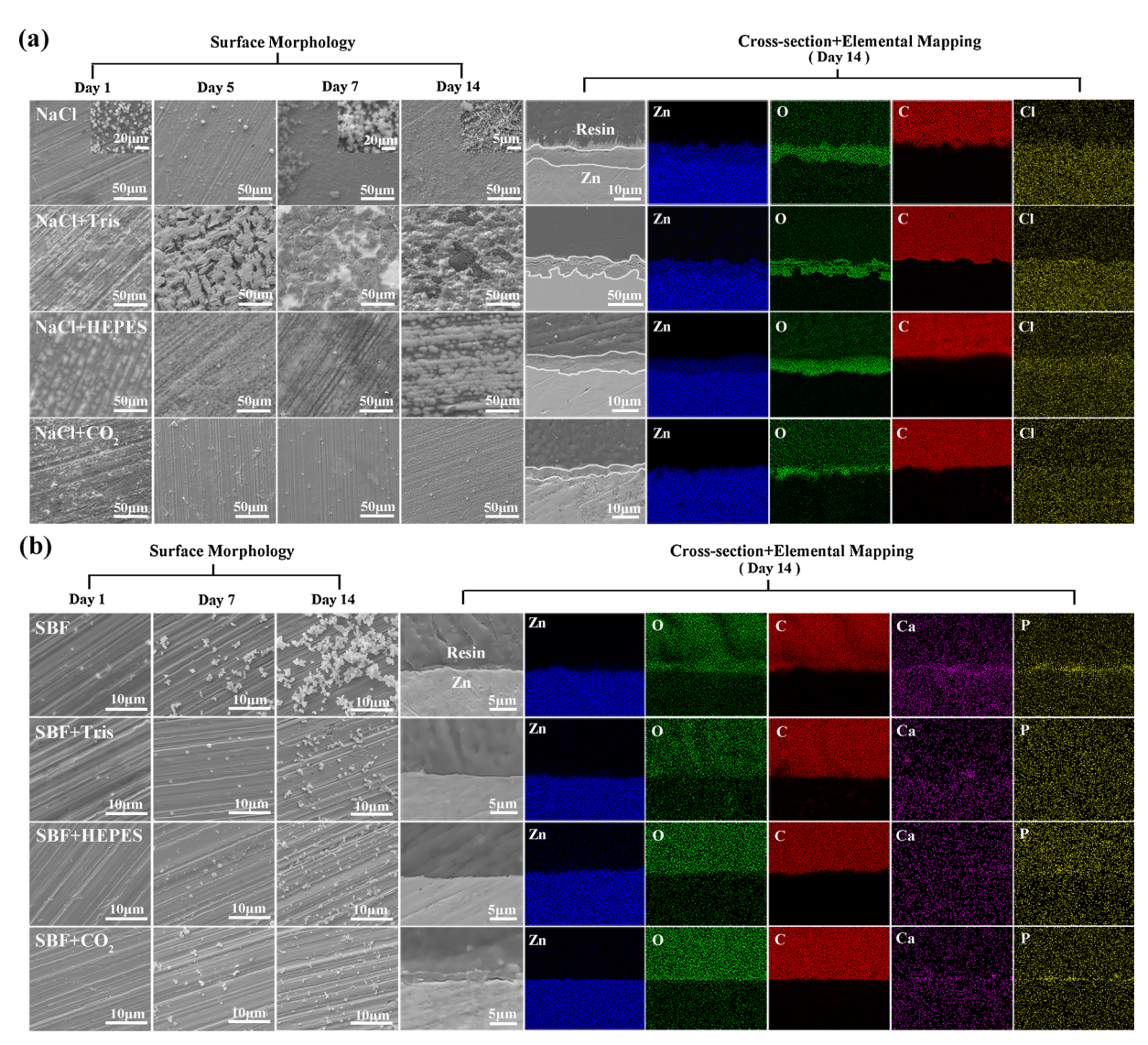


Fig. 1. SEM micrographs showing surface morphology, cross-section and EDS elemental mapping of representative corrosion interface of pure Zn after 14 days of immersion in (a) four 0.9% NaCl solutions and (b) four SBFs.

Table 2
Results of EDS analysis of pure Zn in four 0.9% NaCl solutions (at. %).

	Zn	О	Cl	С
0.9% NaCl solution				
Day 1- layer	78.2	21.8	-	_
Day 1- globular corrosion product	12.5	58.6	0.5	28.4
Day 14- layer	38.6	47.0	1.6	12.8
0.9% NaCl solution buffered with Tris-H	Cl-			
Day 7- layer	25.5	60.0	1.6	12.9
Day 7- white corrosion product	27.0	51.9	0.4	20.7
Day 14- layer	23.5	49.9	0.7	25.9
Day 14- black corrosion product	43.1	48.6	0.8	7.5
0.9% NaCl solution buffered with HEPES	S			
Day 1- layer	13.6	62.4	_	24.0
Day 14- layer	13.6	63.9	_	22.5
0.9% NaCl solution buffered with NaHC	O_3/CO_2			
Day 1- layer	28.1	52.1	_	19.8
Day 14- layer	22.7	54.8	_	22.5

exhibited high intensity and the curve fit consisted of two groups, associated with the divalent oxidation state of Ca in the inorganic calcium oxygen compound [55]. The peak of Ca 2p3/2 in the range of 347.3–347.6 eV [56] and the peak of P 2p at 133.2 eV indicated the

Table 3Results of EDS analysis of pure Zn in four SBF solutions (at. %).

	Zn	О	С	Ca	P	Mg
SBF						
Day 1- surface	66.2	16.9	13.2	1.6	2.1	-
Day 14- layer	26.0	44.2	20.1	4.5	5.2	-
Day 14- white corrosion product	11.3	52.6	16.1	8.6	8.9	2.5
SBF buffered with Tris-HCl						
Day 1- surface	82.3	17.7	-	-	-	-
Day 14- layer	48.6	39.4	5.4	2.0	4.6	-
Day 14- white corrosion product	6.6	66.6	13.1	4.9	8.8	-
SBF buffered with HEPES						
Day 1- surface	90.7	9.3	-	-	-	-
Day 14- layer	51.2	38.7	3.2	2.3	4.6	-
Day 14- white corrosion product	4.9	65.8	12.2	6.5	9.7	0.9
SBF buffered with NaHCO ₃ /CO ₂						
Day 1- surface	92.6	7.4	-	-	-	-
Day 14- layer	63.0	26.0	5.9	2.1	3.0	-
Day 14- white corrosion product	8.8	58.1	16.4	7.4	7.9	1.4

formation of calcium phosphate [57], and the peak of P 2p at 133.93 eV was ascribed to $Zn_3(PO_4)_2 \cdot 4H_2O$ [58].

To summarize, ZnO and $\rm Zn_5(OH)_8Cl_2\cdot 4H_2O$ were formed in four 0.9% NaCl solutions, and extra $\rm Zn_5(CO_3)_2(OH)_6$ was precipitated in

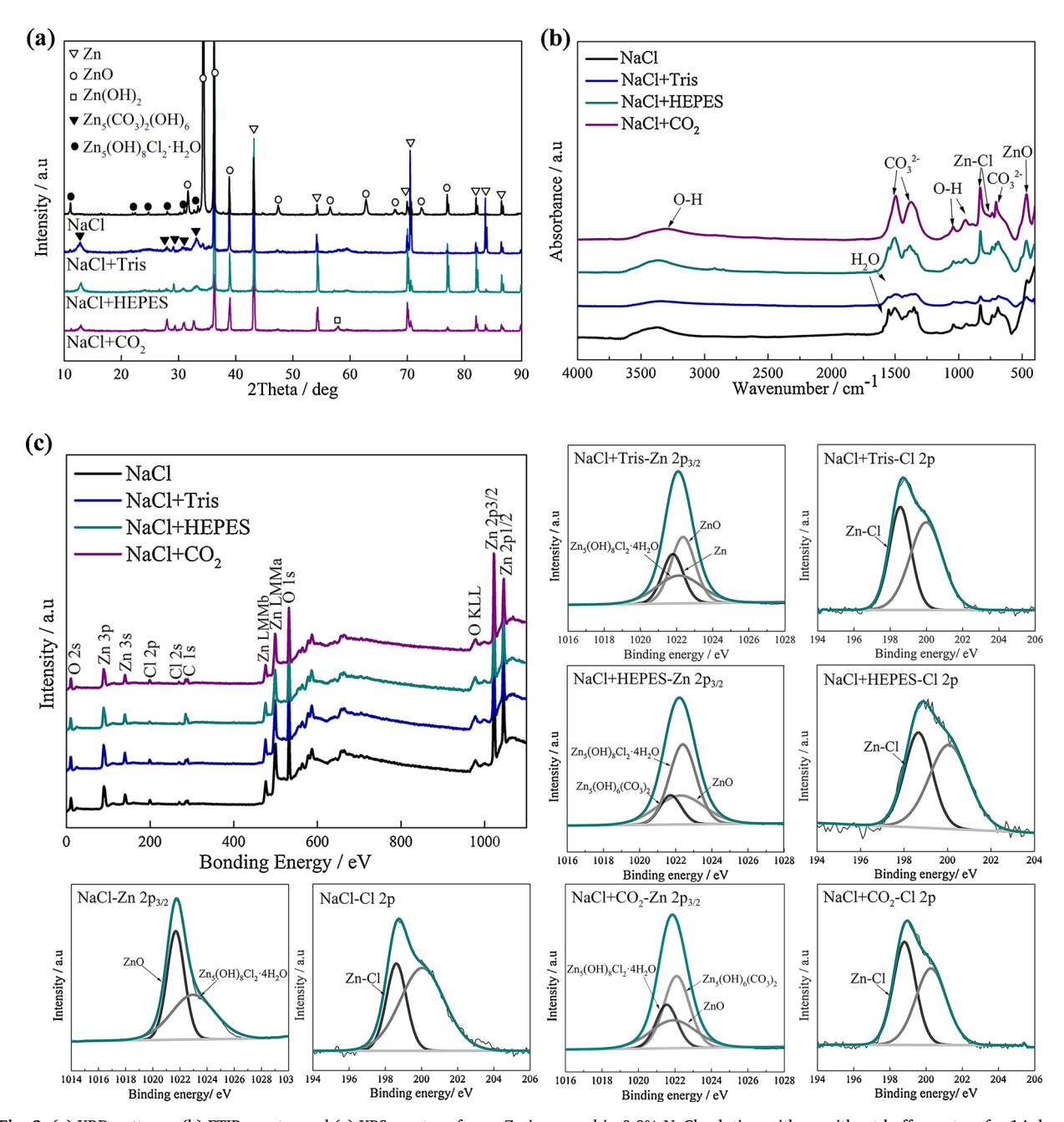


Fig. 2. (a) XRD patterns, (b) FTIR spectra and (c) XPS spectra of pure Zn immersed in 0.9% NaCl solution with or without buffer system for 14 days.

buffered solutions. In three buffered SBFs, ZnO, $\rm Zn_3(PO_4)_2\cdot 4H_2O$ and $\rm Ca_3(PO_4)_2$ were main corrosion products, and $\rm Zn_5(CO_3)_2(OH)_6$ precipitated in NaHCO₃/CO₂ buffered SBF. In SBF, the corrosion product with precise stoichiometry was ZnO, and a thin layer of $\rm Ca_3(PO_4)_2$ covered on the surface, which was thick enough to hinder the excitation of underlaying Zn and therefore finite information about zinc compounds can be presented by XPS.

3.3. Immersion experiments

3.3.1. Change of solution pH in the presence of buffers

The change in solution pH of four NaCl solutions as a function of time is shown in Fig.4a. In NaCl solution, pH increased abruptly after 3 h and dropped instantly. Afterwards, the pH increased with time and reached 10.0 after 14 days. In the presence of buffer system, solution pH was significantly depressed. In NaCl solution with Tris-HCl, pH exhibited the lowest value after 6 h and spawned a continuous increase

thereafter. In the presence of HEPES, solution pH was almost constant and controlled in the range of 7.36-7.40 after 2 days. With the introduction of NaHCO₃/CO₂, the pH was adjusted unceasingly and displayed values ranging from 7.47 to 7.52.

In Fig. 4b, the pH of buffer-free SBF fluctuated all the time and reached the highest value at 8.29. The solution pH of Tris-HCl and HEPES buffered SBF decreased initially and went up later. Solution pH was maintained within a narrow band around the desired pH (7.38–7.43) with Tris-HCl present, and in HEPES buffered SBF, it was maintained at 7.50–7.66. In NaHCO₃/CO₂ buffered SBF, the pH was continuously adjusted and sustained at the range of 7.50-7.54.

3.3.2. Concentration of Zn^{2+} in the presence of buffers

The concentration of ${\rm Zn}^{2+}$ ions in diluted solutions is presented in Fig. 5. In general, ${\rm Zn}^{2+}$ accumulated in the solution and its concentration increased with time. In four NaCl solutions, the release of ${\rm Zn}^{2+}$ was substantially promoted by Tris-HCl and inhibited by

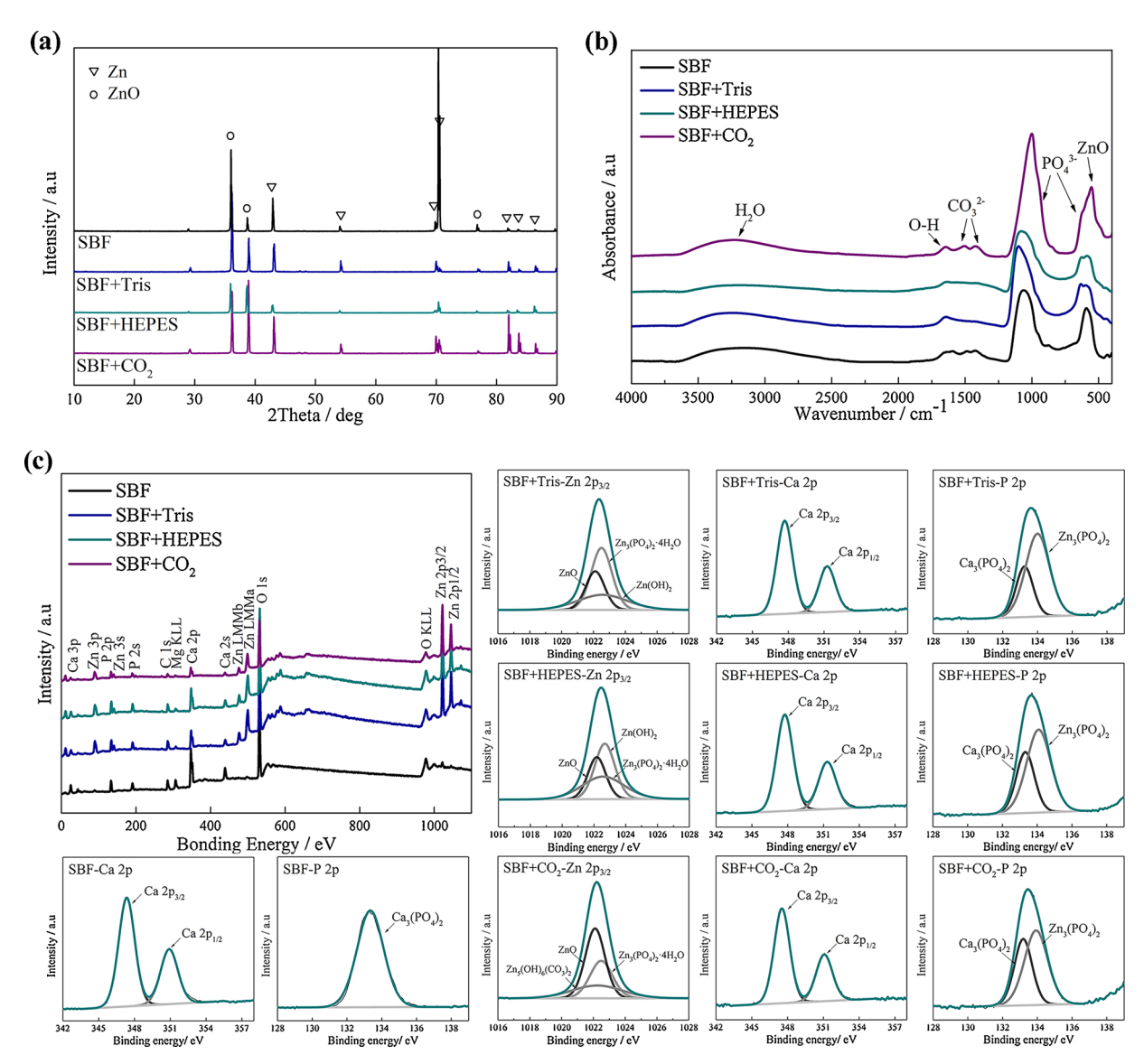


Fig. 3. (a) XRD patterns, (b) FTIR spectra and (c) XPS spectra of pure Zn immersed in SBF with or without buffer system for 14 days.

Table 4FTIR analysis of corrosion product after 14 days of immersion.

Wave number (cm ⁻¹)	Assignments	Reference	
350-600	ZnO	[45]	
560-580	v_4 mode of PO_4^{3-}	[52]	
719, 898	stretching vibration mode of Cl	[44]	
829	v ₂ mode of CO ₃ ²⁻	[40]	
1000-1140	v ₄ mode of PO ₄ ³⁻	[6,52]	
1300-1550	ν ₃ mode of CO ₃ ²⁻	[42,43]	
1595	deformation vibration of water molecules	[40]	
3300-3500	O-H stretching vibrations	[41]	
735, 906, 1037	vibration of Zn-O-H in Zn ₅ (OH) ₈ Cl ₂ ·4H ₂ O	[40]	

 ${
m NaHCO_3/CO_2}$. Unexpectedly, in the presence of Tris-HCl, the concentration of ${
m Zn^{2+}}$ declined after 14 days. In HEPES buffered NaCl solution, the concentration of ${
m Zn^{2+}}$ ion was comparable to that in NaCl solution after 1 day and then fell far behind.

In SBF corrosion media, the release of $\mathrm{Zn^{2+}}$ was greatly elevated by buffer systems. The increase in $\mathrm{Zn^{2+}}$ concentration induced by $\mathrm{NaHCO_3/CO_2}$ was the weakest among three buffers, and HEPES induced the fastest degradation of pure Zn. Moreover, the concentration of $\mathrm{Zn^{2+}}$ in buffer-free and Tris-HCl buffered SBF was relatively lower in

Table 5Results obtained from deconvoluted XPS spectra of Zn 2p3/2, Cl 2p, Ca 2p3/2, P 2p.

Element	Binding energy (eV)	Compound	Reference	
Zn 2p3/2	1021.8	Zn ₅ (OH) ₈ Cl ₂ ·4H ₂ O	[50,51]	
	1022.0-1022.2	ZnO	[46,47]	
	1022.2-1022.4	$Zn_5(CO_3)_2(OH)_6$	[46,48]	
	1022.5	$Zn_3(PO_4)_2\cdot 4H_2O$	[53,54]	
	1022.6-1022.8	$Zn(OH)_2$	[46]	
	1023.0	$Zn_5(OH)_8Cl_2\cdot 4H_2O$	[49]	
Cl 2p	198.6	$Zn_5(OH)_8Cl_2\cdot 4H_2O$	[50]	
	200.6	Na-Cl	[49]	
Ca 2p3/2	347.3-347.6	Ca-P	[56]	
P 2p	133.2	Ca-P	[57]	
	133.93	$Zn_3(PO_4)_2\cdot 4H_2O$	[58]	

comparison to the counter-NaCl solution. In contrast, HEPES and NaHCO $_3$ /CO $_2$ introduced higher amount of Zn^{2+} in SBF than NaCl solution as immersion prolonged.

3.3.3. Weight loss and corrosion rate of pure Zn in the presence of buffers Fig. 5 also presents the weight loss of pure Zn and derived corrosion rates in eight electrolytes. The mass loss of specimens in each solution

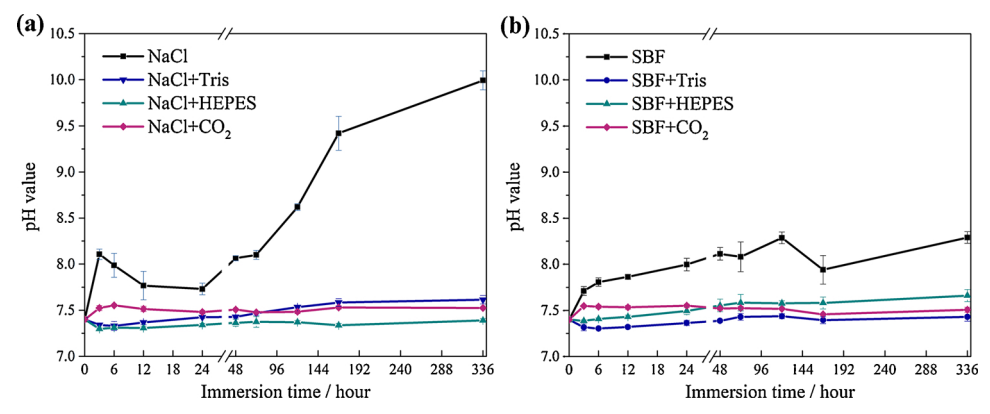


Fig. 4. pH changes of (a) 0.9% NaCl solution and (b) SBF with or without buffer system during 14 days of immersion.

increased with time. In HEPES and NaHCO $_3$ /CO $_2$ buffered NaCl, as well as Tris-HCl buffered SBF, pure Zn exhibited decreased degradation rate with time. In the rest electrolytes, the corrosion rate fluctuated during the whole immersion. In four NaCl solutions, the average degradation rate of 14 days manifested in the following decreasing order: Tris-HCl > NaCl > HEPES > NaHCO $_3$ /CO $_2$. With respect to SBF corrosion media, pure Zn experienced higher weight loss in buffered solutions, in which the degradation rate was raised by a factor as high as ten. The average corrosion rate during 14 days of immersion in SBF and SBF with Tris-HCl, HEPES and NaHCO $_3$ /CO $_2$ was about 0.005 mm·yr $^{-1}$, 0.040 mm·yr $^{-1}$, 0.082 mm·yr $^{-1}$ and 0.037 mm·yr $^{-1}$, respectively.

3.4. Electrochemical measurements

3.4.1. Open circuit potential

Fig. 6 shows the open circuit potential (OCP) as a function of time during 3600 s of immersion in eight electrolytes. In Fig. 6a, the overall OCP decreased with the addition of buffer system, signifying the loss of surface stability. In buffer-free and HEPES buffered NaCl solution, OCP was elevated to more positive values initially. A suddenly drop in OCP took place then, which might correspond to the breakdown of the surface film [59]. Afterwards, OCP tended to stabilize and increased marginally in NaCl solution. In contrast, multiple fluctuations in the potential was demonstrated with HEPES addition, implying the metastable surface breakdown [35]. In Tris-HCl buffered NaCl solution, OCP fluctuated continuously and increased slowly, which was reported to be related to the strong active dissolution due to buffering of Tris-HCl [60]. In NaHCO₃/CO₂ buffered NaCl solution, the OCP was stabilized at about -1.06 V for a while and abruptly declined then. The positive shift of potential during the subsequent immersion was observed, which was likely originated from the deposition of corrosion products on the surface [26].

As shown in Fig. 6b, the corrosion tendency of pure Zn in four SBFs was determined. The OCP values were quite close in four electrolytes, and decreased slightly as a whole with buffer systems added. The changes of OCP in four SBFs also exhibited similar tendency that it shifted to positive value shortly after immersion and displayed downward trend later. After that, fluctuations in the potential took place, indicating the deposition of protective corrosion product [35] and the localized breakdown of surface film [61]. The corrosion tendency in four groups of SBFs was therefore seemingly alike during the early stage of immersion, while it varied significantly in four NaCl solutions.

3.4.2. Potentiodynamic polarization

The potentiodynamic polarization test was performed to provide thermodynamic and kinetic information about Zn degradation [36]. Only pure charge transfer controlled current can be acceptable as true Tafel data [26]. In this study, several experimental polarization curves did not exhibit linear Tafel regions and hence the corrosion current

density was estimated by Tafel extrapolation of the extensive linear region in cathodic or anodic branch of polarization curves. The corrosion potential (E_{corr}), current density (i_{corr}) and estimated corrosion rate (P_i) are listed in Table 6.

In Fig. 7a, the potentiodynamic polarization curves for pure Zn in NaCl solutions are demonstrated. In the presence of buffer systems, the corrosion potential drifted towards negative direction, especially for NaHCO3/CO2 case, signifying the possibly accelerated degradation in the very beginning [62]. For pure Zn in 0.9% NaCl solution, its cathodic curve was composed of several cathodic reactions [63]. Buffered with HEPES and NaHCO₃/CO₂, the cathodic process altered as the cathodic current changed smoothly and approximately linearly. In the case of Tris-HCl, pure Zn displayed faster cathodic reactions and a peak appeared in the cathodic current curve, which might be ascribed to reduction of ZnO [63]. Moreover, the kinetics of anodic reactions in three buffered NaCl solutions varied from NaCl solution. The anodic parts demonstrated a narrow passivation-like protection region and then accelerated to high dissolution rate, denoting the formation and subsequent breakage of the passive film [64]. Moreover, in the presence of NaHCO₃/CO₂, the passivity of corrosion product layer was enhanced as pure Zn exhibited lower anodic dissolution rate [65]. The corrosion rate of pure Zn in four NaCl solutions was calculated based on the cathodic current curve. It turned out that pure Zn degraded slowest in NaCl solution and corrosion rates in three buffered NaCl solutions were comparable.

Fig. 7b presents the potentiodynamic polarization curves of Zn in four SBFs. The electrode exhibited similar curve shapes in four electrolytes, and the cathodic current curve constituted several cathodic reactions. A passive-like region appeared in the anodic current curve and was accompanied by a breakdown point [29], which implied the rupture of protective film [34]. In the presence of Tris-HCl, the corrosion potential increased and both cathodic and anodic curve drifted towards higher current. With HEPES present, pure zinc experienced higher cathodic dissolution rate, reflecting the facilitated cathodic reaction [25]. In NaHCO₃/CO₂ buffered SBF, the corrosion potential shifted negatively and manifested the lowest value. Regarding pure Zn in four SBFs, the corrosion rate was derived from the anodic current curve and reduced as follows: Tris-HCl > HEPES > NaHCO₃/CO₂ > SBF.

3.4.3. Electrochemical impedance spectroscopy

In order to gain a better insight into the electrochemical corrosion processes involved in eight electrolytes, electrochemical impedance spectroscopy was performed. In principle, the impedance response depends on the electrode controlled kinetics [62] and encompasses several sub-processes such as mass transfer, charge transfer, coupling of interfacial reactions, diffusion and intermediate adsorption steps [66]. It's theorized that the individual sub-process could be deduced through comprehensive analysis.

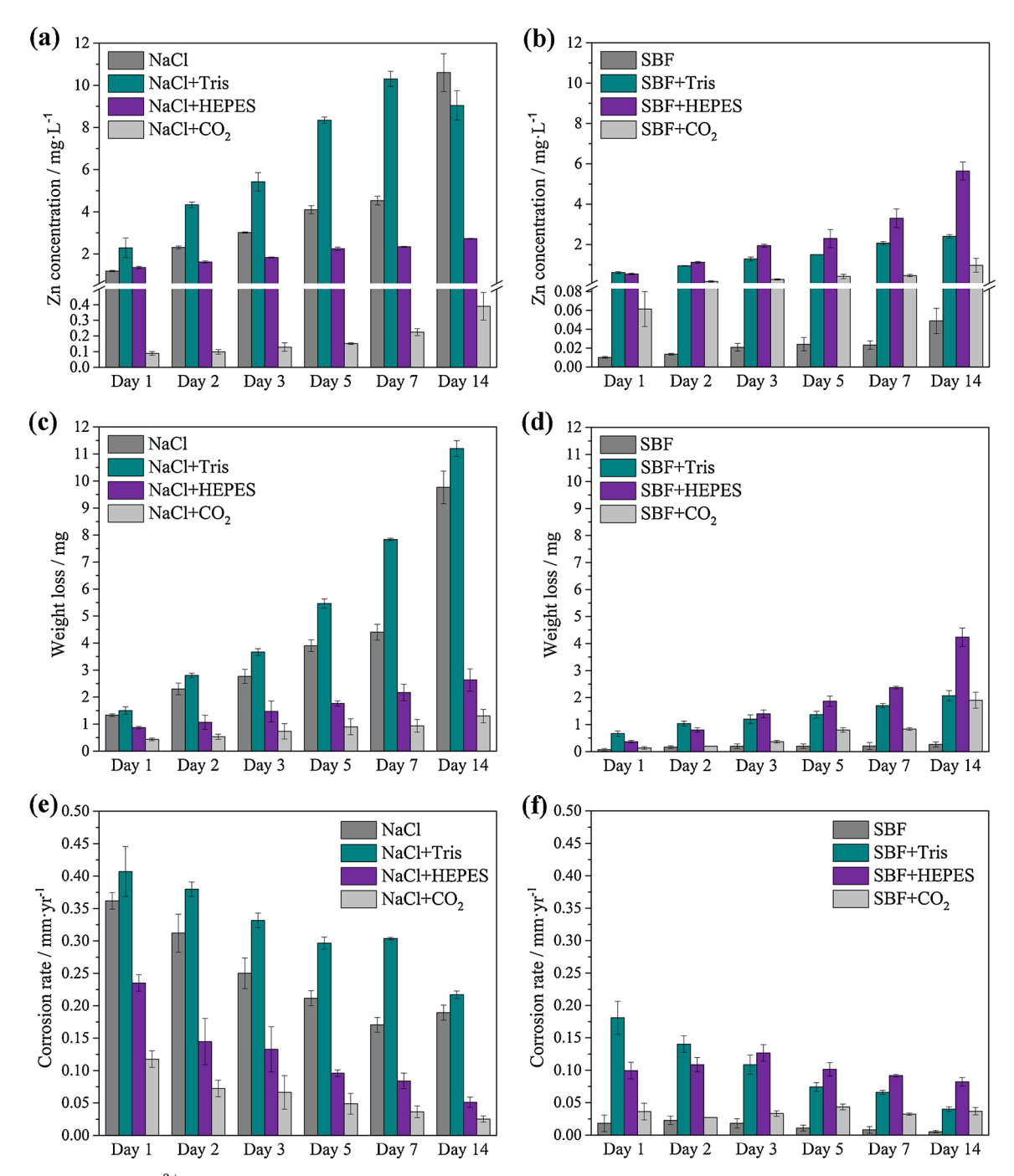


Fig. 5. (a, b) concentration of Zn^{2+} , (c, d) weight loss and (e, f) corrosion rate of pure Zn during 14 days of immersion in 0.9% NaCl solution and SBF with or without buffer system.

The EIS spectra of pure Zn exposed to buffered and non-buffered NaCl solutions are shown in Fig. 8a. The initial degradation behaviour of pure Zn was elucidated since the EIS test was conducted after 1 h of open-circuit exposure. With the addition of buffer system, the diameter of nyquist plot decreased. In buffer-free, HEPES and NaHCO $_3$ /CO $_2$ buffered NaCl solution, the nyquist plot was comprised of two capacitive loops. The semicircle at high frequency was attributed to the faradaic charge transfer process and the one at low frequency represented corrosion product layer [67]. In Tris-HCl buffered NaCl solution, the impedance response manifested an inductive loop appeared at middle frequency. The dissolution of zinc might proceed via adsorbed Zn(I) and Zn(II) intermediates [68] and the inductive behaviour was characteristic for the redeposited Zn. Moreover, the dissolution–deposition

exchange reaction gave rise to active sites for dissolution and the corrosion rate was prone to increase [66]. In comparison to NaCl corrosion media, the nyquist plot demonstrated enlarged dimension in four SBFs, as depicted in Fig. 8b. With or without buffer system, the nyquist plot of pure Zn in SBF exhibited similar patterns and different diameters, revealing the same corrosion processes at the electrode/electrolyte interface but distinct corrosion resistance. In addition, two distinguished time constants were corresponding to two capacitive loops. The capacitive loop at high frequency was associated with charge transfer process and electrochemical double layer. The capacitive loop at low frequency was assigned to the passive film covered on the surface.

In order to obtain further information from the EIS measurements, the plot of pure Zn in Tris-HCl buffered NaCl solution was interpreted

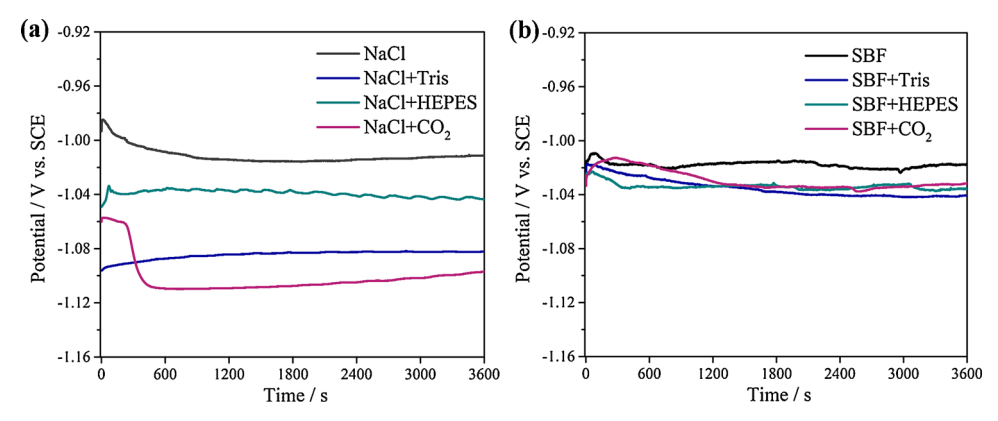


Fig. 6. Open circuit potential of pure Zn immersed in (a) 0.9% NaCl solution and (b) SBF with or without buffer system.

Table 6Electrochemical parameters of PDP curves in eight electrolytes.

	E _{corr} / V vs. SCE	$i_{\rm corr}$ / ($\mu \text{A·cm}^{-2}$)	P _i / (mm/year)
NaCl	-1.034	14.835	0.221
NaCl + Tris-HCl	-1.109	46.368	0.690
NaCl + HEPES	-1.110	45.367	0.675
$NaCl + CO_2$	-1.183	45.429	0.676
SBF	-1.036	2.917	0.043
SBF + Tris-HCl	-1.024	4.172	0.062
SBF + HEPES	-1.076	3.779	0.056
$SBF + CO_2$	-1.109	3.201	0.048

by the equivalent circuit (a2) in Fig. 8a. The spectra in the rest electrolytes was fitted with the same equivalent circuits (a1) and (b1). To better fit the experimental data, constant phase element (CPE) is utilized in place of capacitance to compensate the non-homogeneity as factors like surface roughness and heterogeneities contribute to non-ideal capacitive behaviour. The CPE is given by the following equation:

$$Z_{CPE} = Q^{-1}(j\omega)^{-n} \tag{2}$$

where $-1 \le n \le 1$, Z_{CPE} is the CPE impedance ($\Omega \cdot cm^2$), Q is a constant ($\Omega \cdot cm^2 \cdot s^n$), j is the imaginary number and ω is the angular frequency. Note that n=1 corresponds to the capacitance, a resistor yields n=0, an inductor yields n=-1 and a Warburg element yields n=0.5.

The estimated impedance parameters are listed in Table 7 and the EEC physical interpretation was elaborated as follows: $R_{\rm s}$ represents the electrolyte resistance between the working and reference electrodes. $R_{\rm ct}$ and CPE $_{\rm 1}$ refer to the charge transfer resistance and the electric double layer capacity at the metal/electrolyte interface. $R_{\rm f}$ and CPE $_{\rm 2}$ correspond to the resistance and capacitance of the corrosion product layer. L and $R_{\rm L}$ describe the inductance and inductance resistance due to the adsorption of intermediate species. Usually, the impedance in the low

frequency end of spectrum is interpreted as polarization resistance and inversely proportional to the corrosion rate [67]. The polarization resistance $R_{\rm p}$ can be obtained by the sum of $R_{\rm f}$ and $R_{\rm ct}$. Hence, the corrosion resistance of pure Zn during the early immersion stage in 0.9% NaCl solution diminished in the presence of buffer systems, and the polarization resistance $R_{\rm p}$ in SBFs decreased as follows: SBF > NaHCO₃/CO₂ > Tris-HCl > HEPES.

4. Discussion

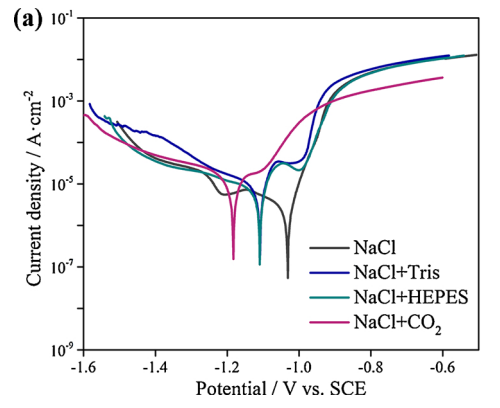
4.1. Corrosion mechanism of pure Zn in 0.9% NaCl solution and SBF

In this study, 0.9% NaCl solution and SBF were used as the corrosion media to investigate the impact of inorganic ions on the functioning of buffer systems and their synergy on the degradation behaviour of pure Zn. Ultimately, the immersion test and electrochemical experiments unveiled the discrepancies of degradation behaviour and demonstrated the corrosion mechanism of pure Zn in eight electrolytes. The schematic diagrams of the corrosion process involved are shown in Figs. 9 and 10.

Several studies have been carried out concerning the corrosion behaviour of zinc in NaCl solution and SBF [7,8]. The corrosion of Zn was claimed to proceed via two partial reactions in both corrosion media. The reduction of oxygen was the dominated cathodic reaction and the anodic reaction was the dissolution of zinc [11,49]. Simultaneous increase in $\rm Zn^{2+}$ and $\rm OH^-$ contributed to the formation of $\rm Zn(OH)_2$, which transformed into more thermodynamically stable ZnO then [6]. The $\rm OH^-$ elevated the pH successively, and at very active cathodic sites, solution pH was high enough for the formation of zincate ions while the consumption of $\rm OH^-$ in turn lowered the pH.

$$O_2 + H_2O + 4e^- \rightarrow 4OH^-$$
 (3)

$$Zn \rightarrow Zn^{2+} + 2e^{-} \tag{4}$$



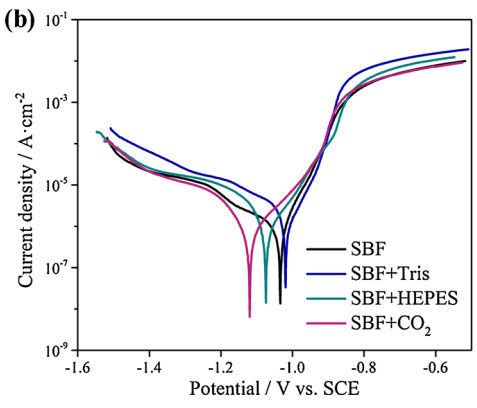


Fig. 7. Potentiodynamic polarization curves of pure Zn immersed in (a) 0.9% NaCl solution and (b) SBF with or without buffer system.

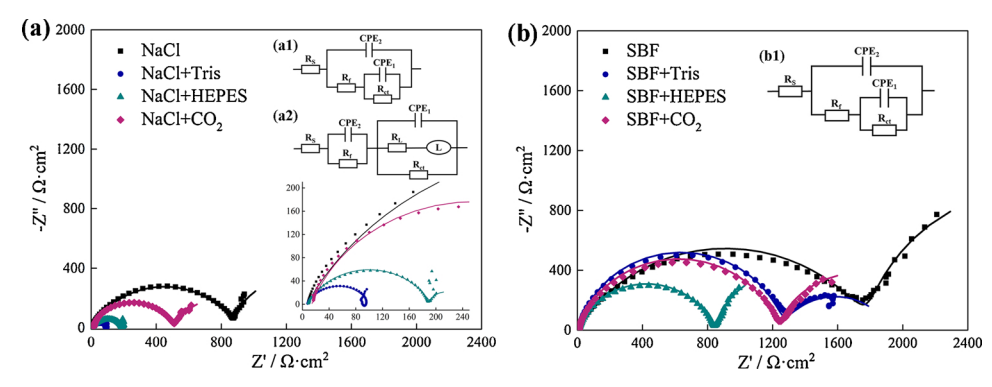


Fig. 8. Nyquist plots and fitting results (lines) of pure Zn in (a) 0.9% NaCl solution and (b) SBF with or without buffer system, and (a1, a2, b1) corresponding electric equivalent circuits used for fitting the experimental impedance spectra.

$$Zn^{2+} + 2OH^{-} \rightarrow Zn(OH)_{2}$$
 (5)

$$Zn(OH)_2 \rightarrow ZnO + H_2O \tag{6}$$

$$Zn(OH)_2 + 2OH^- \rightarrow Zn(OH)_4^{2-}$$
 (7)

In 0.9% NaCl solution, pH value far exceeded the physiological range. The Cl⁻ migrated to anodic sites and the simonkolleite was precipitated [49]. A large quantity of OH⁻ was released and raised pH value remarkably. The layer of corrosion product formed on the surface, inhibiting the further dissolution of pure Zn. Besides, the oxygen reduction caused a local increase in pH values and non-uniform corrosion proceeded over the surface [49]. As immersion time prolonged, pure Zn exhibited more general corrosion pattern and corrosion rate increased mildly after 14 days.

$$5Zn(OH)_2 + 2Cl^- + H_2O \rightarrow Zn_5(OH)_8Cl_2 \cdot H_2O + 2OH^-$$
 (8)

According to FTIR spectra, carbonates were precipitated on the sample surface during the immersion. Actually, the existence of hydrozincite has been reported during the exposure of Zn in 0.6 M NaCl solution [49]. As the immersion test was conducted in a 50 mL plastic tube in this study, there was limited amount of air. The $\rm CO_2$ was therefore so minor to form enough carbonates detectable for XRD.

In SBF, the pH increased with time and deviated from the pH level in physiological environment after 14 days. Inorganic ions such as ${\rm Ca^{2^+}}$, ${\rm HPO_4^{2^-}}$, ${\rm HCO_{3^-}}$ and ${\rm Mg^{2^+}}$ at the anode/electrolyte interface lead to the precipitation of ZnO and ${\rm Zn_3(PO_4)_2\cdot 4H_2O}$ [69], as well as a thin layer of ${\rm Ca_3(PO_4)_2}$ covered on the very surface. The corrosion resistance got improved and pure Zn degraded much slower in SBF.

$$3Zn^{2+} + 2HPO_4^{2-} + 2OH_1 + 2H_2O \rightarrow Zn_3(PO_4)_2 \cdot 4H_2O$$
 (9)

$$3Ca^{2+} + 2PO_4^{3-} \rightarrow Ca_3(PO_4)_2$$
 (10)

Interestingly, the thickness of corrosion product layer formed in 0.9% NaCl solution and SBF was barely comparable, but the degradation of pure Zn got tremendously restrained in SBF. Since the concentrations of Cl⁻ and Na⁺ in two solutions were close, the improved corrosion resistance was likely originated from inorganic ions like Ca²⁺, HPO₄²⁻ and Mg²⁺. The passive films formed in two solutions obtained distinct compositions and various degrees of compactness, and thus may affect the dissolution process differently [69], since the oxidation product film containing simple oxides and chloride species was found insufficient of protection [70], and calcium phosphate were recognized as effective cathodic inhibitors for metals in previous studies [27]. Accordingly, the involvement of inorganic ions in SBF solution could retard the dissolution of pure Zn effectively.

4.2. The dependence of pure Zn degradation on buffer system and corrosion media

4.2.1. Corrosion mechanism of pure Zn in the presence of Tris-HCl

With the introduction of Tris-HCl, the OH- generated from the reduction of oxygen can be quickly consumed by bonded H^+ in Tris-HCl. The increase of pH in NaCl solution was depressed but still exceeded 7.6 after 14 days. In contrast, pH value of SBF was effectively controlled and exhibited acceptable values in human body. It turned out that the buffer capacity of Tris-HCl buffer system differed in two corrosion media.

(11)

Table 7The fitted results of electrochemical impedance spectra of pure Zn in eight electrolytes.

	$R_{\rm s}~(\Omega\cdot{\rm cm}^2)$	$R_{\rm ct} \ (\Omega \cdot {\rm cm}^2)$	$R_{\rm f} (\Omega \cdot {\rm cm}^2)$	$R_{\rm L} (\Omega \cdot {\rm cm}^2)$	CPE_1-Q $(\Omega^{-1}\cdot s^n\cdot cm^{-2})$	CPE ₁ -n	CPE_2 -Q (Ω^{-1} ·s ⁿ ·cm ⁻²)	CPE ₂ -n	L (Ω ·cm ⁻²)
NaCl	6.5	612.4	888.5	_	1.01E-05	0.71	1.01E-02	0.99	_
NaCl + Tris	7.6	92.9	111.3	646.2	1.00E-01	0.98	3.80E-05	0.75	5605.1
NaCl + HEPES	8.2	48.1	183.6	_	3.14E-05	0.73	5.96E-02	0.90	-
$NaCl + CO_2$	14.1	665.6	489.6	_	2.98E-06	0.80	5.28E-03	0.71	-
SBF	6.6	2153.5	1808.5	_	6.57E-06	0.69	2.27E-03	0.92	-
SBF + Tris	9.2	652.7	1256.5	_	1.11E-06	0.88	9.19E-04	0.76	_
SBF + HEPES	9.8	1058.1	830.7	_	2.16E-06	0.82	5.01E-03	0.85	_
$SBF + CO_2$	8.5	979.1	1226.8	-	1.77E-06	0.84	2.82E-03	0.84	-

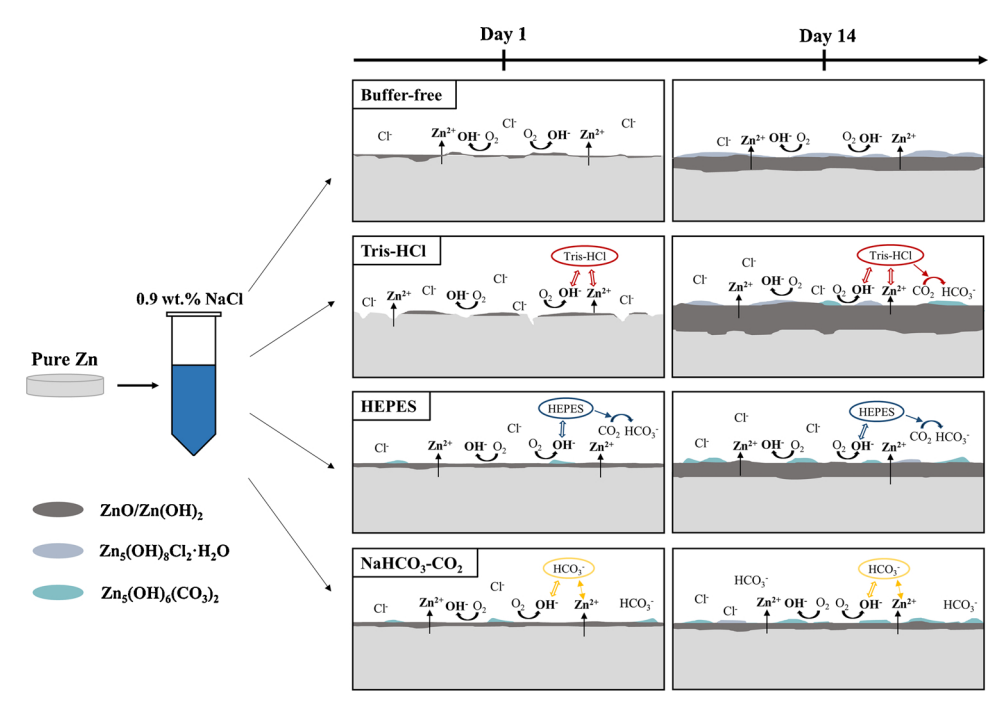


Fig. 9. Schematic illustration of corrosion process involved in four 0.9% NaCl solutions.

During the early immersion stage in NaCl solution, Tris-HCl depleted OH^- and accelerated the oxidation of Zn. Active reactions involving adsorbed intermediates took place in the electrode/electrolytes interface. The surface stability of pure Zn diminished, resulting in negatively shifted corrosion potential and shrunken polarization resistance R_p . The precipitation of corrosion product was suppressed, thus, the dissolution of Zn aggravated and localized corrosion commenced all over the surface. In consequence, pure Zn presented increased degradation rate with time. Likewise, in Tris-HCl buffered NaCl solution, the stable corrosion product layer was absent on the surface of Mg and the dissolution exacerbated [60]. As immersion time extended, the buffer capacity weakened due to the consumption of Tris-HCl [34].

Large quantity of corrosion product was formed and the concentration of ${\rm Zn}^{2+}$ declined after 14 days. The formation of hydrozincite was encouraged since the alkalization was restrained. A thick layer of corrosion product covered the sample surface and the corrosion rate decreased. In Tris-HCl buffered SBF, the formation of corrosion product was inhibited and the polarization resistance $R_{\rm p}$ receded in comparison to SBF. With prolonged immersion, corrosion product was formed and the corrosion rate declined.

$$CO_2 + 2OH^- \rightarrow CO_3^{2-} + H_2O$$
 (12)

$$CO_3^{2-} + H_2O \rightarrow HCO_{3-} + OH-$$
 (13)

$$5\text{Zn}(\text{OH})_2 + 2\text{HCO}_3^- + 2\text{H}^+ \rightarrow \text{Zn}_5(\text{CO}_3)_2(\text{OH})_6 + 4\text{H}_2\text{O}$$
 (14)

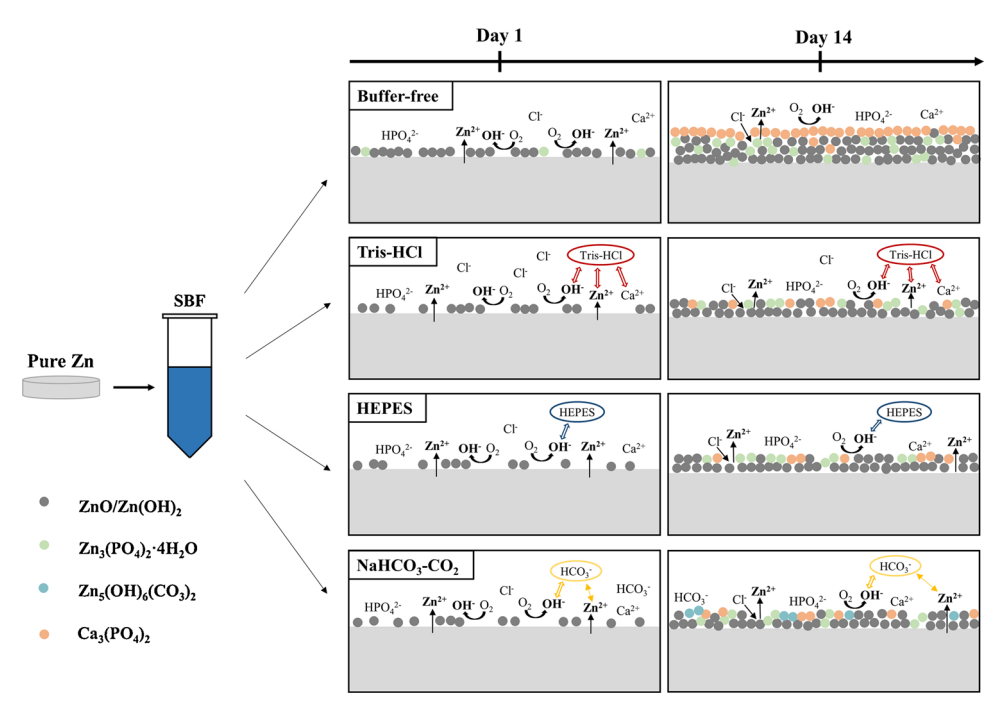


Fig. 10. Schematic illustration of corrosion process involved in four SBFs.

It was claimed that the strong interaction between Tris and dissolved cations or corrosion product caused the activation of sample surface [60]. The light complexation was found between Tris and Zn²⁺ [71], which might transport Zn²⁺ ions from the interface into bulk solution and subsequently delay the formation of a mass transportlimiting solid film [70]. The corrosion of pure Zn was likely to be facilitated, and it can be conjectured that the absent corrosion product during the initial immersion might be associated with the weak ZnL complex. Additionally, the HCl component of the buffer system introduced a large quantity of Cl⁻ [72], which might contribute to pits corrosion and have the detrimental effect on the passivity. As for SBF corrosion media. Tris-HCl was also reported to prevent the precipitation of HPO₄²⁻, HCO₃⁻, SO₄²⁻ and H₂PO₄- [34], and the complexes formed between Tris and Ca²⁺ retarded the deposition of calcium salt [72]. The dissolution of pure Zn was therefore stimulated, but the acceleration of Zn degradation was less promoted by Tris-HCl in SBF compared to NaCl solution.

4.2.2. Corrosion mechanism of pure Zn in the presence of HEPES

HEPES is a zwitterionic buffer and typically contained an acid and base [27]. It could neutralize an excess number of $\mathrm{H^+}$ or $\mathrm{OH^-}$ in the solution and provide a relative neutral environment. In NaCl solution, the buffer range of HEPES was 7.35 to 7.39. In HEPES buffered SBF, solution pH reached 7.66 after 14 days. The buffer ability of HEPES relied on the corrosion media.

During the initial stage of immersion in NaCl solution, the stabilization of the interface was prevented by HEPES due to the limited growth of corrosion products. Pure Zn manifested decreased corrosion potential and polarization resistance. After 1 day, a highly protective film was formed on the surface and inhibited the dissolution of underlying metal effectively. The corrosion resistance got improved and corrosion rate reduced. $\rm Zn_5(CO_3)_2(OH)_6$ was identified but more detailed explanations on the nature of the corrosion product layer was outside the scope here. In SBF, the deposition of corrosion product was inhibited and the dissolution of pure Zn was encouraged. There was insignificant difference among the surface morphology of samples in three buffered SBF but pure Zn demonstrated the highest corrosion rate with HEPES added.

Unlike Tris, HEPES would not form complexes with neither Zn²⁺ nor Ca²⁺, hence the complexation of HEPES can be ignored [73,74]. Nonetheless, it was reported that the addition of HEPES significantly increased the ionic strength of the EBSS, reduced the ion activity largely and restrained the formation of insoluble salt such as phosphate and carbonate on the magnesium surface. Pure Mg exhibited a higher corrosion rate in EBSS because of HEPES [29]. In this study, due to the existence of inorganic ions like Mg²⁺, HPO₄²⁻, HCO₃- and SO₄²⁻, HEPES functioned differently. Its buffer ability changed and corrosion behaviour of pure Zn varied in two solution. In HEPES buffered NaCl solution, the passivating film restrained the Zn dissolution. In contrast, HEPES might raise the ion strength in SBF, inhibit the deposition of corrosion product and eventually caused the acceleration of Zn degradation.

4.2.3. Corrosion mechanism of pure Zn in the presence of NaHCO₃/CO₂

The carbonic acid was formed when released ${\rm CO_2}$ was dissolved in the solution. ${\rm H_2CO_3}$ was in equilibrium with ${\rm HCO_3}^-$ and ${\rm NaHCO_3/CO_2}$ buffer system was established. The pH of ${\rm NaHCO_3/CO_2}$ buffered NaCl solution and SBF was close. Its buffer capacity was seemingly the least dependent on corrosion media among three buffer systems.

$$CO_2 + H_2O \Leftrightarrow H_2CO_3 \Leftrightarrow HCO_3^- + H^+$$
 (15)

$$5Zn^{2+} + 2HCO_3^- + 8OH^- \rightarrow Zn_5(CO_3)_2(OH)_6 + 2H_2O$$
 (16)

Due to inhibited increase in pH, the generation of corrosion product was retarded initially and the surface suffered the loss of stability. $NaHCO_3/CO_2$ lowered the corrosion potential and polarization

resistance of pure Zn in NaCl solution. Nevertheless, the compact corrosion product layer was generated on the surface since the first day. Along with increased ${\rm HCO_3}^-$ concentration, massive ${\rm Zn_5(CO_3)_2(OH)_6}$ was preferred to precipitate, which possessed superior passivity than simple oxides and chloride species [70]. Thus, the corrosion product layer was thinnest among four NaCl solutions after 14 days but demonstrated the highest protectivity, and the dissolution of pure Zn was suppressed noticeably. In SBF, the deposition of corrosion product was restrained by NaHCO₃/CO₂ and the corrosion rate increased. ${\rm Zn_5(CO_3)_2(OH)_6}$ was precipitated, which was absent in Tris – HCl and HEPES buffered SBF and the concrete composition of carbonate was unclear in buffer-free SBF.

Despite similar solution pH, the degradation performance of pure Zn varied in two solutions and the average corrosion rate of 14 days was higher in SBF. It was deduced that during the initial immerison stage, inorganic ions like ${\rm Ca^{2}}^+$, ${\rm HPO_4}^{2-}$, ${\rm HCO_3}^-$ and ${\rm Mg^{2}}^+$ delayed the degradation of pure Zn in buffered SBF. With prolonged immersion, the layer in buffered NaCl solution became more compact and provided enhanced protection, while corrosion product deposition was still inhibited in buffered SBF. Pure Zn therefore degraded faster in buffered SBF during subsequent immersion.

4.3. The comparative study of three buffer systems in SBF

4.3.1. The influence on the Ca-P precipitation

In this work, the calcium phosphate rich layer was formed on the sample surface after 14 days of immersion in buffer-free SBF. In contrast, with the addition of buffer systems, the amount of calcium phosphates diminished. In fact, the formation of calcium phosphate phases was common in cardiovascular and bone implants, and it was a sign to evaluate the biocompatibility of material as tight chemical bonds between implants and the living bone can be formed through it [23]. It's generally acknowledged that the alkalization of solution could encourage the generation of calcium phosphate [35]. In Fig. 4, reduced pH value was displayed in three buffered SBFs, which was highly likely to prevent the Ca-P salts precipitation from taking place. In addition, the light complexation was found between Ca²⁺ and Tris [72], which might lower the concentration of free Ca2+ and further hindered the formation of Ca-P salts in Tris-HCl buffered SBF [74]. As for HEPES buffered SBF, the complexes of HEPES with Ca²⁺ were unlikely to form when isolated [74], therefore the lessened calcium phosphates precipitation might be primarily related to the low pH level [35]. Referring to previous studies, Tris and HEPES also showed negative influence on the precipitation of Ca-P salts on Mg in Dulbecco's modified Eagle's medium (DMEM) [35]. Moreover, it was theorized that an increase in CO2 partial pressure could reduce the driving force for calcium phosphate precipitation and low pH values gave rise to increased number of free Ca²⁺ ion, which meant to stimulate the deposition of calcium phosphate [74]. However, in the NaHCO3/CO2 buffered SBF, the stability of calcium phosphate was compromised by low pH, and the amount of calcium phosphate declined consequently.

4.3.2. The ability to mimic the in vivo environment

Till now, the in vivo performance of pure zinc has been widely studied through several animal models and at different time points to evaluate the potential as endovascular stents or orthopaedic implants. Although there are still some arguments on the corrosion mechanism of Zn in the physiological environment, the most part of which has been revealed. Concerning the degradation behaviour of pure zinc at the very early stage in vivo, much information can be referred to.

Bowen et al. [2] studied the in vivo performance of pure Zn wire in the murine artery and unveiled a degradation rate of $0.012\,\mathrm{mm\cdot yr}^{-1}$ during 1.5 months of exposure. A compact layer of corrosion product formed after 4.5 months was composed of zinc oxide and zinc carbonate, as well as a calcium/phosphorus phase on the exterior surface. The zinc carbonate was considered as an intermediate phase at this time

as several zinc minerals were more thermodynamically stable than it. Nonetheless, after residing in the artery for 12 and 20 months, the corrosion product layer was still recognized as a mixture of ZnO, calcium/phosphorous and zinc carbonate [5]. Later, Yang et al. [6] proposed the degradation mechanism of pure zinc stents implanted in the abdominal aorta of rabbit. During 1 month of implantation, pure zinc degraded at 0.03 mm·yr⁻¹ and underwent a uniform corrosion mode. The layer of corrosion product was mainly composed of ZnO, amorphous Zn₃(PO₄)₂ and polycrystalline Zn₃(PO₄)₂·4H₂O. After 6 months, an outer layer of corrosion product rich in Ca-P was formed and no zinc carbonates appeared during the whole process. Moreover, Bowen et al. [75] found the layer of corrosion product on high grade zinc strip after implantation in the abdominal agrta of rats for 1.5 months was primarily composed of Zn and O, while the outer zone was rich in calcium and phosphorus. In addition, Yang et al. [12] investigated the degradation performance of pure Zn in the femoral condyle of rats and the corrosion product was characterized by layered structure after 8 weeks. The inner layer consisted of oxidized constituents and the outer layer, besides C, O and Zn, also contained Ca and P, which can be distinguished even after 4 weeks.

It's said that a close and effective simulation of in vivo conditions required the similar corrosion rate, corrosion product and corrosion morphology [18]. In this work, pure Zn experienced an extremely low corrosion rate at 0.005 mm·yr⁻¹ during 14 days of immersion in bufferfree SBF. The layered structure corrosion product was identified and the outer layer was primarily composed of Ca-P salts. Clearly, the corrosion rate failed to match that during artery remodelling or bone fracture fixation. Moreover, the advanced appearance of calcium phosphate was inconsistent with that in artery, but correlated with the observation as orthopaedic implant applications [12] since SBF was designed for bone environment originally [23]. Nevertheless, buffer-free SBF was still an inappropriate pseudo-physiological solution as a result of delayed degradation rate and increased pH values. The addition of buffer systems inhibited the formation of calcium phosphate and adjusted the pH values noticeably. The corrosion rate in HEPES buffered SBF was, however, as high as $0.082\,\mathrm{mm\cdot yr^{-1}}$ and pH range slightly exceeded the ideal values. Hence, this combination might not be suitable for mimicking both physiologic environments. In contrast, in the presence of Tris-HCl and NaHCO₃/CO₂, the average corrosion rate of pure Zn during 14 days of immersion was $0.040\,\mathrm{mm\cdot yr^{-1}}$ and $0.037\,\mathrm{mm\cdot yr^{-1}}$, respectively. These values were comparable to that of 1-month implantation in rabbit artery, which was about 0.03 mm·yr⁻¹ and displayed a downward trend with time [6]. The solution pH can be effectively adjusted by two buffers while the pH range of NaHCO3/CO2 slightly exceeded 7.50. Notably, zinc carbonate was formed in NaHCO3/CO2 buffered SBF, which was absent in HEPES and Tris-HCl buffered SBF. It should be noted that the formation of carbonates, as well as the zinc phosphates during artery remodelling was a controversy for now. Different corrosion product was characterized in vivo and the variations might come from different animal models, implantation sites, material purity and processing methods [2,5,6,75]. On the contrary, the reduced but still existed Ca-P salts had the good correspondence with bone environments. But since the precise degradation rate of pure Zn in the bone environments was unavailable for now, the practicability of two systems for orthopaedic fixation device was beyond the scope here. Therefore, we reached a provisional conclusion that both Tris-HCl and NaHCO3/CO2 buffered SBF can be adopted to characterize the early stage corrosion behaviour of biodegradation zinc for the vascular stent applications.

4.4. Prospects of in vitro evaluations

In principle, in vitro tests are designed to evaluate the degradation behaviour of materials and identify ones with great potential for costly and time-consuming animal tests subsequently. However, previous studies demonstrated that in vitro corrosion tests in simple simulated body fluids cannot fully predict Zn corrosion in vivo [17]. The uncertainty might have detrimental effect on the further research, at the price of both effort and money. Building an in vitro methodology that can accurately simulate the degradation behaviour in vivo is urgently demanded and has always been the intention of researchers. Considering and evaluating essential factors for the in vivo corrosion and reproducing these factors in vitro are mostly recommended to achieve the goal [18].

For biodegradable magnesium, the step towards a closer simulation of in vivo conditions have obtained some achievements. Influence factors such as solution component, temperature, pH and flow rate have been widely and systematically analysed [18]. The CO₂ buffered Hank's solution showed great promise to mimic the in vivo corrosion behaviour for Mg [32]. However, despite decades of efforts, the cutting-edge studies continue revealing more in-depth information about inorganic ions [72], organic components [76,77] and so on. It's a very broad field of investigation and finding the most appropriate in vitro test environment for magnesium is still in progress. In contrast, the investigation of zinc is in the beginning phase and the academic system is also in embryo. Thus, previous researches on the biodegradable magnesium are valuable and of instructive significance. Nonetheless, the disparity came up that for magnesium corrosion, the pH-control ability of buffer systems was weaker due to the fast dissolution of magnesium and HEPES was likely to complex with Mg²⁺. The CO₂ buffer possessed the advantage of better reflecting physiological conditions over Tris and HEPES [28], inconsistent with the circumstance of Zn. Thus, it's necessary to comment objectively to properly benefit from the research experience in Mg corrosion.

In this study, the importance of solution pH and buffer system, as well as the motivation to build the in vitro methodology for Zn corrosion was proposed and emphasized for the first time. What's more, Tris-HCl or $NaHCO_3/CO_2$ buffered SBF was suggested to characterize the early stage corrosion behaviour of biodegradation zinc. The proposal might not be mature enough but definitely an important step forward. Seeking the best in vitro methodology for Zn corrosion is a long journey, worthwhile and meaningful but still has a long way to go.

5. Conclusions

In this study, the influence of Tris-HCl, HEPES, and $NaHCO_3/CO_2$ on the corrosion behaviour of pure Zn was investigated through immersion tests and electrochemical approaches, and the following conclusions can be drawn:

- (1) The solution pH affected the corrosion product formation and can be effectively adjusted by three buffer systems with different pHcontrol capacity. Inorganic ions in SBF retarded the dissolution of pure Zn and altered the buffer capacity. The synergy of buffer system and inorganic ions contributed to the unique corrosion behaviour of pure Zn in each electrolyte.
- (2) Tris-HCl inhibited corrosion product precipitation and increased corrosion rate in two corrosion media, and severe pits corrosion was induced in NaCl solution. HEPES and NaHCO₃/CO₂ promoted the formation of passive film in NaCl solution and reduced the corrosion rate, while they retarded the deposition of corrosion product in SBF and accelerated the degradation. In SBF, the precipitation of calcium phosphate was suppressed by three buffer systems.
- (3) Regarding the ability to mimicking the in vivo degradation behaviour, Tris-HCl or NaHCO₃/CO₂ buffered SBF was recommended as the appropriate combination to evaluate the biodegradation behaviour of zinc in vitro for vascular stent applications.

Acknowledgements

This work was supported by National Natural Science Foundation of China (Grant No. 51431002 and 51871004) NSFC/RGC Joint Research

Scheme (Grant No. 51661165014), and Peking University Medicine Seed Fund for Interdisciplinary Research (Grant No. BMU2018ME005).

References

- [1] Y.F. Zheng, X.N. Gu, F. Witte, Biodegradable metals, Mater. Sci. Eng. R Rep. 77 (2014) 1–34, https://doi.org/10.1016/j.mser.2014.01.001.
- [2] P.K. Bowen, J. Drelich, J. Goldman, Zinc exhibits ideal physiological corrosion behavior for bioabsorbable stents, Adv Mater 25 (2013) 2577–2582, https://doi. org/10.1002/adma.201300226.
- [3] P.K. Bowen, R.J. Guillory 2nd, E.R. Shearier, J.M. Seitz, J. Drelich, M. Bocks, F. Zhao, J. Goldman, Metallic zinc exhibits optimal biocompatibility for bioabsorbable endovascular stents, Mater. Sci. Eng. C Mater. Biol. Appl. 56 (2015) 467–472, https://doi.org/10.1016/j.msec.2015.07.022.
- [4] R.J. Guillory, P.K. Bowen, S.P. Hopkins, E.R. Shearier, E.J. Earley, A.A. Gillette, E. Aghion, M. Bocks, J.W. Drelich, J. Goldman, Corrosion characteristics dictate the long-term inflammatory profile of degradable zinc arterial implants, ACS Biomater. Sci. Eng. 2 (2016) 2355–2364, https://doi.org/10.1021/acsbiomaterials.6b00591.
- [5] A.J. Drelich, S. Zhao, R.J. Guillory 2nd, J.W. Drelich, J. Goldman, Long-term surveillance of zinc implant in murine artery: surprisingly steady biocorrosion rate, Acta Biomater. 58 (2017) 539–549, https://doi.org/10.1016/j.actbio.2017.05.045.
- [6] H. Yang, C. Wang, C. Liu, H. Chen, Y. Wu, J. Han, Z. Jia, W. Lin, D. Zhang, W. Li, W. Yuan, H. Guo, H. Li, G. Yang, D. Kong, D. Zhu, K. Takashima, L. Ruan, J. Nie, X. Li, Y. Zheng, Evolution of the degradation mechanism of pure zinc stent in the one-year study of rabbit abdominal aorta model, Biomaterials 145 (2017) 92–105, https://doi.org/10.1016/j.biomaterials.2017.08.022.
- [7] Y. Meng, L. Liu, D. Zhang, C. Dong, Y. Yan, A.A. Volinsky, L.-N. Wang, Initial formation of corrosion products on pure zinc in saline solution, Bioact. Mater. (2018), https://doi.org/10.1016/j.bioactmat.2018.08.003.
- [8] L. Liu, Y. Meng, C. Dong, Y. Yan, A.A. Volinsky, L.-N. Wang, Initial formation of corrosion products on pure zinc in simulated body fluid, J. Mater. Sci. Technol. 34 (2018) 2271–2282, https://doi.org/10.1016/j.jmst.2018.05.005.
- [9] Z. Tang, J. Niu, H. Huang, H. Zhang, J. Pei, J. Ou, G. Yuan, Potential biodegradable Zn-Cu binary alloys developed for cardiovascular implant applications, J. Mech. Behav. Biomed. Mater. 72 (2017) 182–191, https://doi.org/10.1016/j.jmbbm. 2017.05.013
- [10] H.R. Bakhsheshi-Rad, E. Hamzah, H.T. Low, M. Kasiri-Asgarani, S. Farahany, E. Akbari, M.H. Cho, Fabrication of biodegradable Zn-Al-Mg alloy: mechanical properties, corrosion behavior, cytotoxicity and antibacterial activities, Mater. Sci. Eng. C Mater. Biol. Appl. 73 (2017) 215–219, https://doi.org/10.1016/j.msec. 2016.11.138
- [11] K. Beaussant Törne, A. Örnberg, J. Weissenrieder, Characterization of the protective layer formed on zinc in whole blood, Electrochim. Acta 258 (2017) 1476–1483, https://doi.org/10.1016/j.electacta.2017.12.018.
- [12] H. Yang, X. Qu, W. Lin, C. Wang, D. Zhu, K. Dai, Y. Zheng, In vitro and in vivo studies on zinc-hydroxyapatite composites as novel biodegradable metal matrix composite for orthopedic applications, Acta Biomater. 71 (2018) 200–214, https:// doi.org/10.1016/j.actbio.2018.03.007.
- [13] Z.B. Tang, H. Huang, J.L. Niu, L. Zhang, H. Zhang, J. Pei, J.Y. Tan, G.Y. Yuan, Design and characterizations of novel biodegradable Zn-Cu-Mg alloys for potential biodegradable implants, Mater. Des. 117 (2017) 84–94, https://doi.org/10.1016/j. matdes.2016.12.075.
- [14] C. Wang, H.T. Yang, X. Li, Y.F. Zheng, In vitro evaluation of the feasibility of commercial Zn alloys as biodegradable metals, J. Mater. Sci. Technol. 32 (2016) 909–918. https://doi.org/10.1016/j.imst.2016.06.003.
- [15] Y.Q. Chen, W.T. Zhang, M.F. Maitz, M.Y. Chen, H. Zhang, J.L. Mao, Y.C. Zhao, N. Huang, G.J. Wan, Comparative corrosion behavior of Zn with Fe and Mg in the course of immersion degradation in phosphate buffered saline, Corros. Sci. 111 (2016) 541–555, https://doi.org/10.1016/j.corsci.2016.05.039.
- [16] K. Torne, M. Larsson, A. Norlin, J. Weissenrieder, Degradation of zinc in saline solutions, plasma, and whole blood, J. Biomed. Mater. Res. B Appl. Biomater. 104 (2016) 1141–1151. https://doi.org/10.1002/jbm.b.33458.
- [17] G. Katarivas Levy, J. Goldman, E. Aghion, The prospects of zinc as a structural material for biodegradable implants—a review paper, Metals 7 (2017) 402, https://doi.org/10.3390/met7100402.
- [18] S. Johnston, M. Dargusch, A. Atrens, Building towards a standardised approach to biocorrosion studies: a review of factors influencing Mg corrosion in vitro pertinent to in vivo corrosion, Sci. China Mater. 61 (2017) 475–500, https://doi.org/10. 1007/s40843-017-9173-7.
- [19] C.M.H. Ferreira, I.S.S. Pinto, E.V. Soares, H.M.V.M. Soares, (Un)suitability of the use of pH buffers in biological, biochemical and environmental studies and their interaction with metal ions – a review, RSC Adv. 5 (2015) 30989–31003, https:// doi.org/10.1039/c4ra15453c.
- [20] P.K. Bowen, E.R. Shearier, S. Zhao, R.J. Guillory 2nd, F. Zhao, J. Goldman, J.W. Drelich, Biodegradable metals for cardiovascular stents: from clinical concerns to recent Zn-Alloys, Adv. Healthc. Mater. 5 (2016) 1121–1140, https://doi.org/10. 1002/adhm.201501019.
- [21] S. Thomas, N. Birbilis, M.S. Venkatraman, I.S. Cole, Corrosion of Zinc as a Function of pH, CorrosionUs 68 (2012) 160–166, https://doi.org/10.5006/1.3676630.
- [22] S. Johnston, Z.M. Shi, A. Atrens, The influence of pH on the corrosion rate of high-purity Mg, AZ91 and ZE41 in bicarbonate buffered Hanks' solution, Corros. Sci. 101 (2015) 182–192, https://doi.org/10.1016/j.corsci.2015.09.018.
- [23] T. Kokubo, H. Takadama, How useful is SBF in predicting in vivo bone bioactivity? Biomaterials 27 (2006) 2907–2915, https://doi.org/10.1016/j.biomaterials.2006.

01 017

- [24] M.A. Metrick, J.E. Temple, G. MacDonald, The effects of buffers and pH on the thermal stability, unfolding and substrate binding of RecA, Biophys. Chem. 184 (2013) 29–36, https://doi.org/10.1016/j.bpc.2013.08.001.
- [25] F. El-Taib Heakal, O.S. Shehata, N.S. Tantawy, Degradation behaviour of AZ80E magnesium alloy exposed to phosphate buffer saline medium, Corros. Sci. 86 (2014) 285–294, https://doi.org/10.1016/j.corsci.2014.06.008.
- [26] F. El-Taib Heakal, A.M. Fekry, M. Abd El-Barr Jibril, Electrochemical behaviour of the Mg alloy AZ91D in borate solutions, Corros. Sci. 53 (2011) 1174–1185, https:// doi.org/10.1016/j.corsci.2010.11.040.
- [27] N.T. Kirkland, J. Waterman, N. Birbilis, G. Dias, T.B. Woodfield, R.M. Hartshorn, M.P. Staiger, Buffer-regulated biocorrosion of pure magnesium, J. Mater. Sci. Mater. Med. 23 (2012) 283–291, https://doi.org/10.1007/s10856-011-4517-y.
- [28] M. Schinhammer, J. Hofstetter, C. Wegmann, F. Moszner, J.F. Löffler, P.J. Uggowitzer, On the immersion testing of degradable implant materials in simulated body fluid: active pH regulation using CO2, Adv. Eng. Mater. 15 (2013) 434–441, https://doi.org/10.1002/adem.201200218.
- [29] M.B. Kannan, H. Khakbaz, A. Yamamoto, Understanding the influence of HEPES buffer concentration on the biodegradation of pure magnesium: an electrochemical study, Mater. Chem. Phys. 197 (2017) 47–56, https://doi.org/10.1016/j. matchemphys.2017.05.024.
- [30] J. Walker, S. Shadanbaz, N.T. Kirkland, E. Stace, T. Woodfield, M.P. Staiger, G.J. Dias, Magnesium alloys: predicting in vivo corrosion with in vitro immersion testing, J. Biomed. Mater. Res. B Appl. Biomater. 100 (2012) 1134–1141, https://doi.org/10.1002/jbm.b.32680.
- [31] I. Marco, A. Myrissa, E. Martinelli, F. Feyerabend, R. Willumeit-Romer, A.M. Weinberg, O. Van der Biest, In vivo and in vitro degradation comparison of pure Mg, Mg-10Gd and Mg-2Ag: a short term study, Eur. Cell. Mater. 33 (2017) 90–104, https://doi.org/10.22203/eCM.v033a07.
- [32] N.I. Zainal Abidin, B. Rolfe, H. Owen, J. Malisano, D. Martin, J. Hofstetter, P.J. Uggowitzer, A. Atrens, The in vivo and in vitro corrosion of high-purity magnesium and magnesium alloys WZ21 and AZ91, Corros. Sci. 75 (2013) 354–366, https://doi.org/10.1016/j.corsci.2013.06.019.
- [33] Z. Darzynkiewicz, B. Jacobson, HEPES-buffered media in lymphocyte cultures, Proceedings of the Society for Experimental Biology & Medicine Society for Experimental Biology & Medicine 136 (1971) 387–393, https://doi.org/10.3181/ 00379727-136-35271.
- [34] L.-Y. Cui, Y. Hu, R.-C. Zeng, Y.-X. Yang, D.-D. Sun, S.-Q. Li, F. Zhang, E.-H. Han, New insights into the effect of Tris-HCl and Tris on corrosion of magnesium alloy in presence of bicarbonate, sulfate, hydrogen phosphate and dihydrogen phosphate ions, J. Mater. Sci. Technol. 33 (2017) 971–986, https://doi.org/10.1016/j.jmst. 2017.01.005.
- [35] S. Naddaf Dezfuli, Z. Huan, J.M.C. Mol, M.A. Leeflang, J. Chang, J. Zhou, Influence of HEPES buffer on the local pH and formation of surface layer during in vitro degradation tests of magnesium in DMEM, Prog. Nat. Sci. 24 (2014) 531–538, https://doi.org/10.1016/j.pnsc.2014.08.009.
- [36] N.T. Kirkland, N. Birbilis, M.P. Staiger, Assessing the corrosion of biodegradable magnesium implants: a critical review of current methodologies and their limitations, Acta Biomater. 8 (2012) 925–936, https://doi.org/10.1016/j.actbio.2011.11. 014.
- [37] L.-Y. Li, B. Liu, R.-C. Zeng, S.-Q. Li, F. Zhang, Y.-H. Zou, H.G. Jiang, X.-B. Chen, S.-K. Guan, Q.-Y. Liu, In vitro corrosion of magnesium alloy AZ31 a synergetic influence of glucose and Tris, Front. Mater. Sci. 12 (2018) 184–197, https://doi.org/10.1007/s11706-018-0424-1.
- [38] Y. Xin, P.K. Chu, Influence of Tris in simulated body fluid on degradation behavior of pure magnesium, Mater. Chem. Phys. 124 (2010) 33–35, https://doi.org/10. 1016/j.matchemphys.2010.07.010.
- [39] A. Yamamoto, S. Hiromoto, Effect of inorganic salts, amino acids and proteins on the degradation of pure magnesium in vitro, Mater. Sci. Eng. C 29 (2009) 1559–1568, https://doi.org/10.1016/j.msec.2008.12.015.
- [40] J. Winiarski, W. Tylus, B. Szczygieł, EIS and XPS investigations on the corrosion mechanism of ternary Zn–Co–Mo alloy coatings in NaCl solution, Appl. Surf. Sci. 364 (2016) 455–466, https://doi.org/10.1016/j.apsusc.2015.12.183.
- [41] J. Winiarski, W. Tylus, A. Lutz, I. De Graeve, B. Szczygieł, The study on the corrosion mechanism of protective ternary Zn Fe Mo alloy coatings deposited on carbon steel in 0.5 mol dm –3 NaCl solution, Corros. Sci. 138 (2018) 130–141, https://doi.org/10.1016/j.corsci.2018.04.011.
- [42] K. Torne, A. Ornberg, J. Weissenrieder, Influence of strain on the corrosion of magnesium alloys and zinc in physiological environments, Acta Biomater. 48 (2017) 541–550, https://doi.org/10.1016/j.actbio.2016.10.030.
- [43] M. Bitenc, M. Marinšek, Z. Crnjak Orel, Preparation and characterization of zinc hydroxide carbonate and porous zinc oxide particles, J. Eur. Ceram. Soc. 28 (2008) 2915–2921, https://doi.org/10.1016/j.jeurceramsoc.2008.05.003.
- [44] D.Y. Momodu, F. Barzegar, A. Bello, J. Dangbegnon, T. Masikhwa, J. Madito, N. Manyala, Simonkolleite-graphene foam composites and their superior electrochemical performance, Electrochim. Acta 151 (2015) 591–598, https://doi.org/10. 1016/j.electacta.2014.11.015.
- [45] Q. Qu, L. Li, W. Bai, C. Yan, C.-n. Cao, Effects of NaCl and NH4Cl on the initial atmospheric corrosion of zinc, Corros. Sci. 47 (2005) 2832–2840, https://doi.org/ 10.1016/j.corsci.2004.11.010.
- [46] G. Ballerini, K. Ogle, M.G. Barthés-Labrousse, The acid-base properties of the surface of native zinc oxide layers: an XPS study of adsorption of 1,2-diaminoethane, Appl. Surf. Sci. 253 (2007) 6860–6867, https://doi.org/10.1016/j.apsusc.2007.01. 126.
- [47] K. Aramaki, The effect of modification with hydrogen peroxide on a hydrated cerium(III) oxide layer for protection of zinc against corrosion in 0.5M NaCl, Corros.

- Sci. 48 (2006) 766-782, https://doi.org/10.1016/j.corsci.2005.01.014.
- [48] L.S. Dake, D.R. Baer, J.M. Zachara, Auger parameter measurements of zinc-compounds relevant to zinc transport in the environment, Surf. Interface Anal. 14 (1989) 71–75, https://doi.org/10.1002/sia.740140115.
- [49] M. Mouanga, P. Berçot, J.Y. Rauch, Comparison of corrosion behaviour of zinc in NaCl and in NaOH solutions. Part I: Corrosion layer characterization, Corros. Sci. 52 (2010) 3984–3992, https://doi.org/10.1016/j.corsci.2010.08.003.
- [50] J. Duchoslav, R. Steinberger, M. Arndt, T. Keppert, G. Luckeneder, K.H. Stellnberger, J. Hagler, G. Angeli, C.K. Riener, D. Stifter, Evolution of the surface chemistry of hot dip galvanized Zn–Mg–Al and Zn coatings on steel during short term exposure to sodium chloride containing environments, Corros. Sci. 91 (2015) 311–320, https://doi.org/10.1016/j.corsci.2014.11.033.
- [51] J. Duchoslav, M. Arndt, T. Keppert, G. Luckeneder, D. Stifter, XPS investigation on the surface chemistry of corrosion products on ZnMgAl-coated steel, Anal. Bioanal. Chem. 405 (2013) 7133–7144, https://doi.org/10.1007/s00216-013-7099-3.
- [52] A. Ślósarczyk, Z. Paszkiewicz, C. Paluszkiewicz, FTIR and XRD evaluation of carbonated hydroxyapatite powders synthesized by wet methods, J. Mol. Struct. 744-747 (2005) 657–661, https://doi.org/10.1016/j.molstruc.2004.11.078.
- [53] L.P. Kazanskii, E.M. Sokolova, Y.E. Pronin, Adsorption of 1,2,3-benzotriazole on zinc surface from phosphate solution, Prot. Met. Phys. Chem. Surf. 49 (2013) 844–853, https://doi.org/10.1134/s2070205113070101.
- [54] T. Pan, M.H. Ma, F.B. Xin, X.Q. Xin, XPS and AES investigation of nanometer composite coatings of Ni-P-ZnX on steel surface (ZnX = ZnSnO3, Zn-3(PO4)(2), ZnSiO3), Appl. Surf. Sci. 181 (2001) 191–195.
- [55] A.P. Md Saad, R.A. Abdul Rahim, M.N. Harun, H. Basri, J. Abdullah, M.R. Abdul Kadir, A. Syahrom, The influence of flow rates on the dynamic degradation behaviour of porous magnesium under a simulated environment of human cancellous bone, Mater. Des. 122 (2017) 268–279, https://doi.org/10.1016/j.matdes.2017.03.029.
- [56] T. Hanawa, S. Hiromoto, K. Asami, Characterization of the surface oxide film of a Co-Cr-Mo alloy after being located in quasi-biological environments using XPS, Appl. Surf. Sci. 183 (2001) 68–75, https://doi.org/10.1016/S0169-4332(01) 00551.7
- [57] S.Z. Khalajabadi, M.R. Abdul Kadir, S. Izman, M. Marvibaigi, The effect of MgO on the biodegradation, physical properties and biocompatibility of a Mg/HA/MgO nanocomposite manufactured by powder metallurgy method, J. Alloys. Compd. 655 (2016) 266–280, https://doi.org/10.1016/j.jallcom.2015.09.107.
- [58] E.C. Onyiriuka, Zinc phosphate glass surfaces studied by XPS, J. Non. Solids 163 (1993) 268–273, https://doi.org/10.1016/0022-3093(93)91304-L.
- [59] R.C. Zeng, Y. Hu, S.K. Guan, H.Z. Cui, E.H. Han, Corrosion of magnesium alloy AZ31: the influence of bicarbonate, sulphate, hydrogen phosphate and dihydrogen phosphate ions in saline solution, Corros. Sci. 86 (2014) 171–182, https://doi.org/ 10.1016/j.corsci.2014.05.006
- [60] N. Ott, P. Schmutz, C. Ludwig, A. Ulrich, Local, element-specific and time-resolved dissolution processes on a Mg-Y-RE alloy – influence of inorganic species and buffering systems, Corros. Sci. 75 (2013) 201–211, https://doi.org/10.1016/j. corsci.2013.06.003.
- [61] W. Ma, Y. Liu, W. Wang, Y. Zhang, Effects of electrolyte component in simulated body fluid on the corrosion behavior and mechanical integrity of magnesium, Corros. Sci. 98 (2015) 201–210. https://doi.org/10.1016/j.corsci.2015.05.012.
- [62] Y. Xin, K. Huo, H. Tao, G. Tang, P.K. Chu, Influence of aggressive ions on the

- degradation behavior of biomedical magnesium alloy in physiological environment, Acta Biomater. 4 (2008) 2008–2015, https://doi.org/10.1016/j.actbio.2008.05.
- [63] H.J. Flitt, D.P. Schweinsberg, Synthesis, matching and deconstruction of polarization curves for the active corrosion of zinc in aerated near-neutral NaCl solutions, Corros. Sci. 52 (2010) 1905–1914, https://doi.org/10.1016/j.corsci.2010.02.046.
- [64] J.-C. Liu, S. Park, S. Nagao, M. Nogi, H. Koga, J.-S. Ma, G. Zhang, K. Suganuma, The role of Zn precipitates and Cl – anions in pitting corrosion of Sn–Zn solder alloys, Corros. Sci. 92 (2015) 263–271, https://doi.org/10.1016/j.corsci.2014.12.014.
- [65] Y. Song, E.-H. Han, K. Dong, D. Shan, C.D. Yim, B.S. You, Study of the corrosion product films formed on the surface of Mg-xZn alloys in NaCl solution, Corros. Sci. 88 (2014) 215–225, https://doi.org/10.1016/j.corsci.2014.07.034.
- [66] L. Sziraki, E. Szocs, Z. Pilbath, K. Papp, E. Kalman, Study of the initial stage of white rust formation on zinc single crystal by EIS, STM/AFM and SEM/EDS techniques, Electrochim. Acta 46 (2001) 3743–3754, https://doi.org/10.1016/S0013-4686(01)
- [67] M. Mouanga, P. Berçot, Comparison of corrosion behaviour of zinc in NaCl and in NaOH solutions; Part II: electrochemical analyses, Corros. Sci. 52 (2010) 3993–4000, https://doi.org/10.1016/j.corsci.2010.08.018.
- [68] C. Cachet, F. Ganne, G. Maurin, J. Petitjean, V. Vivier, R. Wiart, EIS investigation of zinc dissolution in aerated sulfate medium. Part I: bulk zinc, Electrochim. Acta 47 (2001) 509–518, https://doi.org/10.1016/S0013-4686(01)00740-X.
- [69] E. Mostaed, M. Sikora-Jasinska, J.W. Drelich, M. Vedani, Zinc-based alloys for degradable vascular stent applications, Acta Biomater. 71 (2018) 1–23, https://doi.org/10.1016/j.actbio.2018.03.005.
- [70] T.H. Muster, I.S. Cole, The protective nature of passivation films on zinc: surface charge, Corros. Sci. 46 (2004) 2319–2335, https://doi.org/10.1016/j.corsci.2004. 01.002.
- [71] A. Krezel, W. Maret, The biological inorganic chemistry of zinc ions, Arch. Biochem. Biophys. 611 (2016) 3–19, https://doi.org/10.1016/j.abb.2016.04.010.
- [72] D. Mei, S.V. Lamaka, J. Gonzalez, F. Feyerabend, R. Willumeit-Römer, M.L. Zheludkevich, The role of individual components of simulated body fluid on the corrosion behavior of commercially pure Mg, Corros. Sci. (2018), https://doi. org/10.1016/j.corsci.2018.11.011.
- [73] M. Sokolowska, W. Bal, Cu(II) complexation by "non-coordinating" N-2-hydroxyethylpiperazine-N'-2-ethanesulfonic acid (HEPES buffer), J. Inorg. Biochem. 99 (2005) 1653–1660. https://doi.org/10.1016/j.jiinorgbio.2005.05.007.
- [74] G.M. Platt, I.N. Bastos, M.C. Andrade, G.D.A. Soares, In silico experiments of carbon dioxide atmosphere and buffer type effects on the biomimetic coating with simulated body fluids, Adv. Mater. Phys. Chem. 2 (2012) 239–248, https://doi.org/10. 4236/ampc.2012.24036.
- [75] P.K. Bowen, J.M. Seitz, R.J. Guillory 2nd, J.P. Braykovich, S. Zhao, J. Goldman, J.W. Drelich, Evaluation of wrought Zn-Al alloys (1, 3, and 5 wt % Al) through mechanical and in vivo testing for stent applications, J. Biomed. Mater. Res. B Appl. Biomater. 106 (2018) 245–258, https://doi.org/10.1002/jbm.b.33850.
- [76] R.-Q. Hou, N. Scharnagl, R. Willumeit-Römer, F. Feyerabend, Different effects of single protein vs. Protein mixtures on magnesium degradation under cell culture conditions, Acta Biomater. (2019), https://doi.org/10.1016/j.actbio.2019.02.013.
- [77] T. Li, Y. He, J. Zhou, S. Tang, Y. Yang, X. Wang, Influence of albumin on in vitro degradation behavior of biodegradable Mg-1.5Zn-0.6Zr-0.2Sc alloy, Mater. Lett. 217 (2018) 227–230, https://doi.org/10.1016/j.matlet.2018.01.082.